Characterization, Calibration and Validation of DustIQ PV Cells as Sensor for PV Usable Light.

Sameep Karki

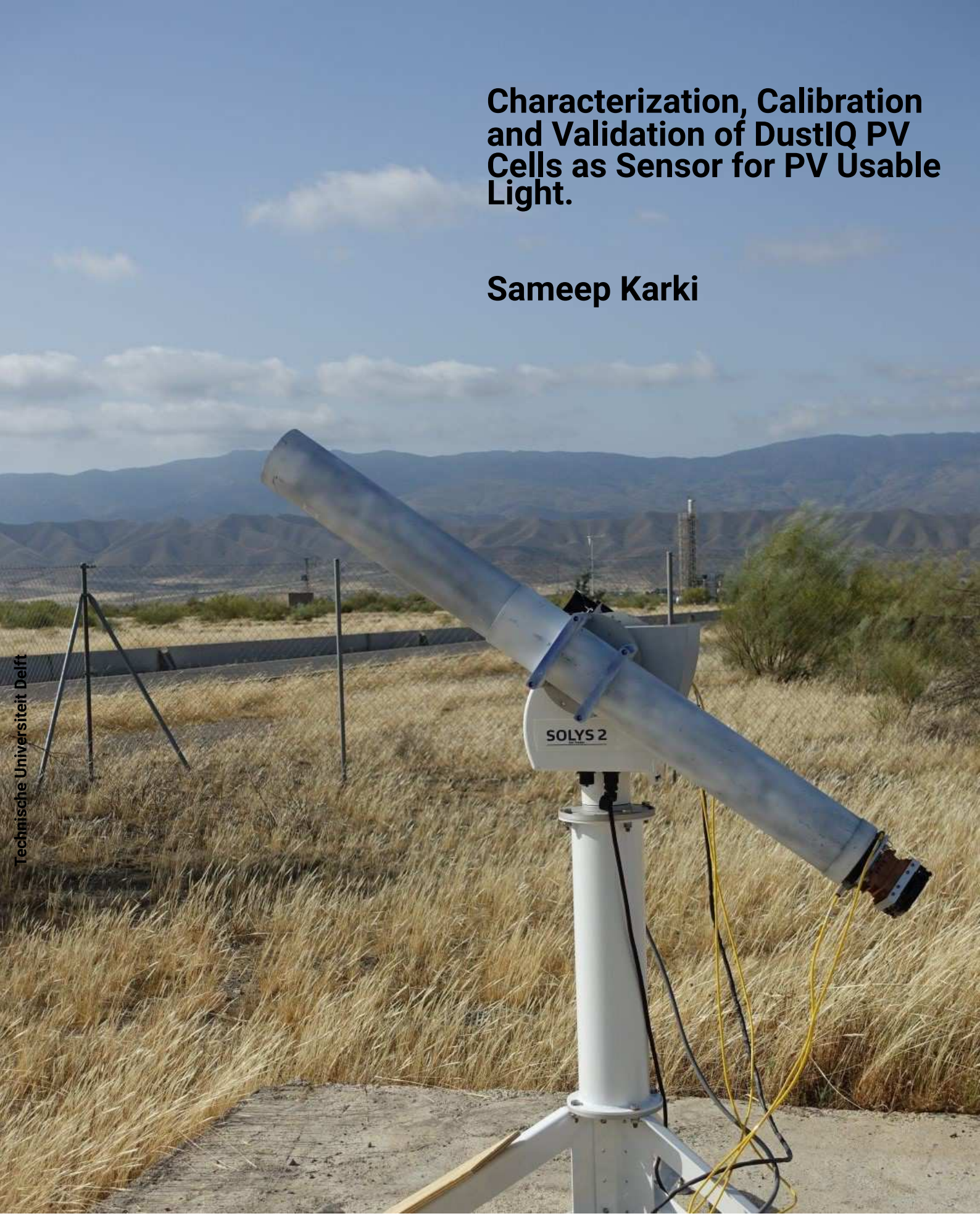

Technische Universiteit Delft

TU Delft

Characterization, Calibration and Validation of DustIQ PV cells as Sensor for PV Usable Light

by

Sameep Karki

to obtain the degree of Master of Science
at the Delft University of Technology,
to be defended publicly on Friday July 05, 2019 at 02:00 PM.

Student number:	4738292	
Supervisor:	Dr. Olindo Isabella	
	Dr. Marc Korevaar	
Thesis committee:	Dr. Olindo Isabella,	TU Delft
	Dr. Marc Korevaar,	Kipp & Zonen
	Dr. Hesan Ziar ,	TU Delft
	Dr. Babak Gholizad,	TU Delft

This thesis is confidential and cannot be made public until July 5, 2021.

TU Delft

Abstract

The growth of Photovoltaic (PV) industry has been overwhelming for the past few years. PV systems suffer from losses due to various factors such as soiling, shading, defects in the systems and many others. Hence continuous monitoring of power generation from PV modules is a necessity to obtain optimal output from the PV systems. The various irradiance sensors available in the market can be useful for continuous monitoring of PV systems all around the globe.

The Dust IQ sensor from Kipp & Zonen has a Mini-PV module on board. The PV module is used for on-site calibration of Dust IQ. The Dust IQ can be made multi-functional by developing the mini- PV module as a PV reference cell. This will help the device to measure soiling and determine performance ratio of the PV systems. The investigation of the calibration procedure of the Mini PV module in DustIQ showed the need for a Primary reference cell. The report describes the design of Primary Reference cell housing, calibration and characterization procedure of PV cell in the Primary reference cell.

There are many sensors available in the market to measure POA irradiance to calculate the performance ratio of PV systems. The prices of these sensors vary according to the design, calibration procedure and characterization conducted. The CMP21 Thermopile Pyranometer from Kipp & Zonen is considered to be one of the most accurate irradiance sensors in the market. In this report, various cost-effective sensors are compared with CMP21 to check the accuracy of the respective sensors. The obtained results showed that cost-effective sensors deviated from the output of the Pyranometers. The silicon pyranometers ( ) underestimates the irradiance with median error bias by -5 W/m^2 (-3%), respectively. For another silicon pyranometer ( ), the bias error is -1 W/m^2 which is significantly lower. The error range for is -8 W/m^2 to 8 W/m^2 (-5% to 5%).

Among all the sensors, the PV reference cell ( ) from has the highest bias error and error range. The error overestimates the irradiance with error ranging from -8 W/m^2 to 22 W/m^2 (-2% to 6%) with a bias of 6 W/m^2. The relative error range is low for due to a huge number of outliers in the data. The dataset of the sensor reduced after the outliers were removed. The cost-effective sensors performance with CMP21 as a reference instrument during varying Air mass (AM) was evaluated. The study exhibited that Silicon Pyranometer performance was close to Pyranometer during varying Air mass while the PV reference cell displayed huge disparity during high Air mass. The silicon pyranometer ( ) performance agreed with the CMP21 performance throughout the measurement period.

Acknowledgements

First of all, I would like to thank Dr. Olindo Isabella for providing me with the opportunity to work on this research project and guiding me throughout the project. I would also like to thank Dr. Marc Korevaar, my daily supervisor for his amazing support, contribution, and guidance towards the project. I would also like to extend my deepest gratitude to Thijs and Denis for their invaluable contribution during the course of this thesis. This work would not have been possible without their insights and suggestions. I am grateful to Dr. Hesan Ziar for guiding me throughout the project. I would also like to thank Mr. Stefaan for helping me with the experiments of the project.

I consider myself fortunate to have had the direct/indirect support of several individuals especially Arturo, Joop, Manish, Pramod, Prinjiya, Sandeep, Seemant and Sharad. I am also grateful to TU Delft and Kipp & Zonen B.V. for providing me with the best environment to grow and learn professionally. Lastly, and most importantly, I want to thank my mom and brother for their constant support and encouragement throughout my life. It is their blessings that always kept me strong in life. Also, I cannot thank my girlfriend enough for her unfailing support.

I want to dedicate this thesis to my late dad, Rajan Karki.

Sameep Karki
Delft, The Netherlands
July, 2019

Contents

List of Figures

List of Tables

1 Introduction

The world is going through an immense transformation from traditional fossil fuels to a reliable and clean source of energy. The imminent problem of climate change due to extreme carbon emissions has a widespread negative effect on the life cycle of the world,and leads to the realization of the instant need for renewable and clean energy. Renewable energy such as solar energy has grown tremendously due to the massive push for sustainable energy technologies to maintain the global temperature by 1.5°C [1].

The huge amount of investments in the research and production of PV technology has led to enormous leap to make the technology affordable and economically viable. The downfall of price to 0.024 USD/kWh during the power purchase agreement in Dubai recently has given more incentive all over the world to shift to sustainable technologies to relieve the budding energy demand [2]. The PV deployment has grown exponentially with global installed capacity capping 508 GW [3].

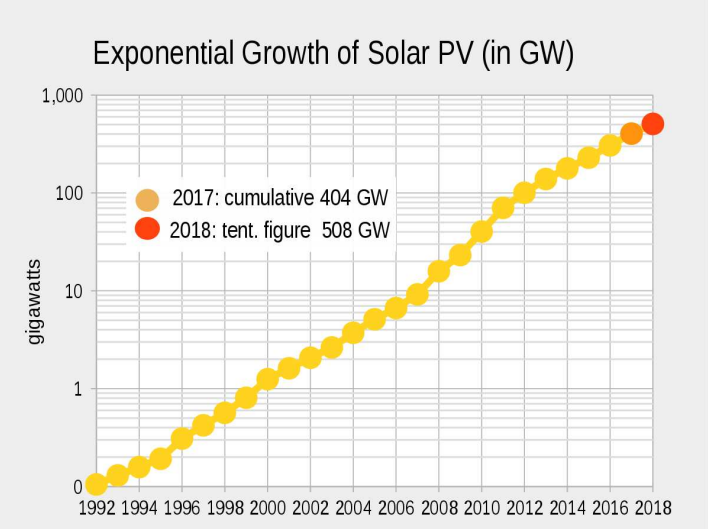

Figure 1.1: Global cumulative PV installation by 2018 [3].

However, the loss in a PV module output is a major problem due to various aspects such as soiling, shading in spite of rapid PV installations. The exhaustive study of system performance to know the amount of losses and attain the maximum conceivable yield from a PV system. This is possible through the continuous monitoring of PV systems with the help of different irradiance sensors available in the market.

1.1. Irradiance sensors

Irradiance is the measurement of solar power incident per unit area. It is expressed as W/m^2. The irradiance device is the instrument which measure the irradiance. The instrument is vital to know the total solar power incident in a certain location, analyze the PV system performances and analyze various losses initiated due to atmospheric condition. The solar spectrum ranges from 150 nm to 4000 nm and the information on the total amount of useful radiation is important for PV system installation and performance evaluation [4]. The different types of irradiance sensors which measures the total useful solar radiation available in the market are described below:

1.1.1. Thermopile Pyranometer

The thermopile pyranometer measures the total useful light incident on the flat earth surface or also known as global horizontal irradiance (GHI). The device also measures Plane of array (POA). It is the technology that measures irradiance from all direction with its dome which has 180°field of view (FOV). The thermal gradient is measured across two areas which are known as hot and cold areas. The temperature difference between the hot and cold area is proportional to irradiance. The device measures have broadband of solar irradiance with wavelength measurement which ranges from 280 nm - 2800nm [5].

1.1.2. Silicon Diode Pyranometer

The Silicon diode pyranometer consists of silicon semiconductor embedded behind the diffuser. The photo-current produced from this semiconductor is proportional to the amount of irradiance. The device only measures the narrow wavelength which ranges from 300 nm- 1100 nm which means the device only measures limited range of solar irradiance [6]. The device measures both GHI and POA.

1.1.3. PV Reference cell

The cell is used to measure the irradiance which can be converted into electricity rather than broadband irradiance. The device resembles the properties of a PV module. The photon incident on the PV reference cell leads to the generation of current which can later be measured as an irradiance. The reference cell angular response, construction and materials used can be same as a PV module which helps in accurate yield prediction of PV module.

(a) Pyranometer

(b)Silicon Pyranometer

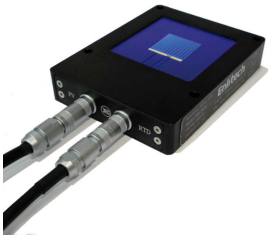

(b)PV Reference cell

Figure 1.2: Different types of Irradiance sensors [5][7]

1.2. Importance of Irradiance sensors

The irradiance sensors are important devices to evaluate the amount of solar irradiance in certain locations, and it also helps to check the useful irradiance in certain location that can be converted into electricity. The performance ratio which can be evaluated using irradiance sensors is discussed below.

1.2.1. Factors influencing performance of PV systems

Performance ratio is the important parameter that can be evaluated with the help of Irradiance sensors. The PV systems operate under different environmental conditions and performance changes with the changes in outdoor conditions. The performance ratio is important to determine the performance of PV systems and the factors effecting the performance. The performance ratio has increased from 70 % in 1990 to 90% to this date according to the study conducted by Fraunhofer [8]. The various factors which influences the Performance ratio are discussed below.

1.2.2. Temperature loss

The power output of the PV cell deviates with the variations in the temperature. The changes in P-V and I-V curve due to the increment of temperature is well documented. The maximum power and efficiency of the PV cell decrease linearly as the temperature increases. The influence of temperature on PV cell performance is represented by the temperature coefficient for maximum power γ [%/ °C].
The I-V and P-V curve gives insight into the temperature dependence of the power output of the PV as shown in cell 1.3.

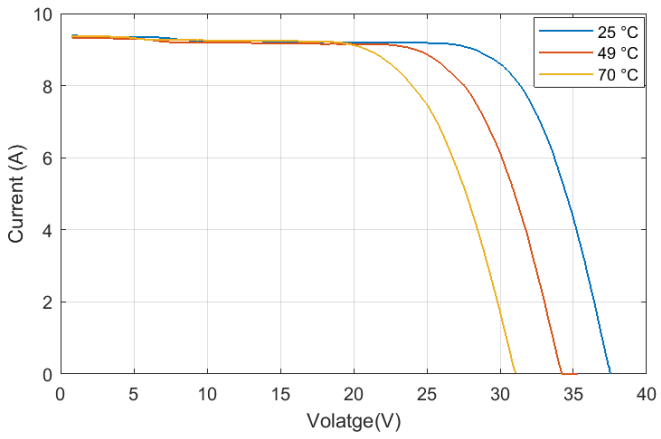

(a) I-V curve

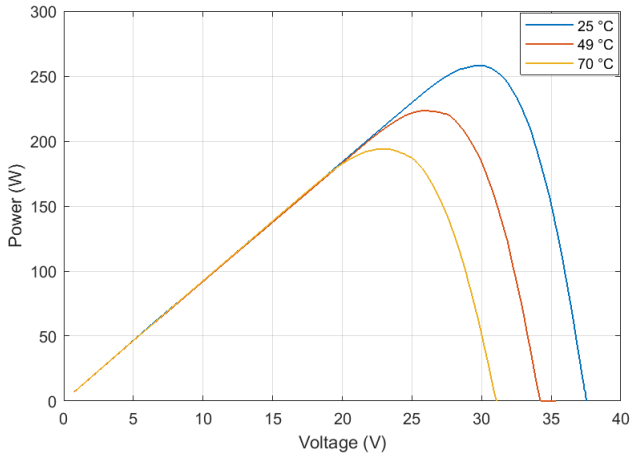

(b) P-V curve

Figure 1.3: Influence of temperature on the characteristic curves of a PV cell [9].

The voltage, current and fill factor are influenced by temperature as the maximum power decreases linearly with increasing temperature. The maximum power can be calculated by [10],

$$P_{MPP} = V_{MPP} \times I_{MPP} = FF \times V_{OC} \times I_{SC} \tag{1.1}$$

Here the subscripts SC, OC, and MPP signify short circuit current, open circuit voltage, and Maximum power point respectively. The $\boldsymbol{V_{OC}}$ of the PV cell is dependent on temperature as it decreases when the temperature increases. The saturation current density $\boldsymbol{J_O}$ increases as the $\boldsymbol{V_{OC}}$ decreases [10]. This is represented by the following equation [10].

$$V_{OC} = \frac{kT}{q} \ln\left(\frac{J_{SC}}{J_0}\right) \tag{1.2}$$

where $\boldsymbol{k}$ is the Boltzmann constant i.e. 1.381×10^{-23} J/K and $\boldsymbol{q}$ is equal to one elementary charge i.e. 1.602×10^{-19} C. As the temperature increases the bandgap of semiconductor device increases resulting in more photogenerated current. Thus it can be inferred that short circuit current density increases slightly as the temperature increases. The slight increase of ($\boldsymbol{J_{SC}}$) is outdone by the drop in open circuit voltage causing the drop in maximum power output of the cell. The efficiency and fill factor of the cell also declines with drop in maximum power output [11].

1.2.3. Effects of Irradiance on PV cell

Irradiance is the amount of power received by earth surface per unit area expressed as Watt per metre square. The irradiance incident on PV cell directly influence the power output of the solar cell. The lack of parameters at different irradiance by manufacturers makes it difficult to determine influence of irradiance on PV cell [10]. The impact of irradiance on PV cell is tricky to analyze than the effect of Temperature. The PV cell power is higher when the irradiance level is more which is illustrated by following equation [10].

$$\eta = \frac{I_{SC} \times V_{OC} \times FF}{G_C \times A_C} \tag{1.3}$$

Where η is the efficiency of the solar cell, A_C is the area of the solar cell, G_C is the irradiance incident on PV cell. The efficiency of the cell decreases with the higher irradiance level.

1.2.4. Transmission loss due to soiling

The soiling of the PV module is one of the major issues leading to lower performance ratio (PR). The location of PV modules installations and environmental conditions at specific regions are the major factors contributing to the soiling of the PV module. The places like Middle east, Asia Pacific, south America were the yield from PV systems is high due to abundant sunlight also sees decrements on yield due to soiling [12]. The soil, dust, smog , snow, pollution due to construction works and industries as well as the growth of micro organisms contributes towards soiling in PV module [13]. The orientation of the PV modules also causes soiling in PV modules. The tilt angle of the PV modules increases as the location shifts away from the equator leading to accumulation of dust at the edges of PV modules [14].
The transmittance of photons declines due to the occurrence of foreign elements on PV module surface which results in lower power output from PV modules [13]. This reduction in transmission of photons due to soiling is referred to as Transmission loss calculated using the following equation [14],

$$T_{loss} = 1 - SR = 1 - \frac{G_S}{G_C} \times 100\% = 1 - \frac{I_{SC,S}}{I_{SC,C}} \times 100\% \tag{1.4}$$

Here, (G_S) and (G_C) are the irradiance of soiled and cleaned module respectively whereas ($I_{SC,S}$) and ($I_{SC,C}$) are current of soiled and cleaned module respectively. The ratio of irradiance of the soiled module to cleaned module or ratio of short circuit current of the soiled and cleaned module is known as soiling ratio [14]. The Transmission loss is an accurate parameter to determine power loss in the module due to soiling. The soiling in the PV modules can be uniform and non- uniform [12]. The uniform soiling is deposition of dust in PV module homogeneously which effects current of the PV module whereas the non-uniform occurs when there

is an accumulation of dust or foreign object in the certain area of PV module which causes partial shading. The partial shading causes considerable effects on the power output of PV cells [15].

Figure 1.4: Soiled and unsoiled module .

a) Commercial Product to determine soiling:

The industries and research facilities are working tirelessly to develop products which can precisely measure the power loss in PV modules due to soiling. The precise and cost effective devices helps to determine soiling behaviour in the PV modules, which can be followed by scheduled cleaning of PV modules. Some of the popular products available in market for soiling measurements are Dust IQ from Kipp & Zonen, Soiling measurements instruments from Atonometrics,PVsoil from ground works and many others. The details on Dust IQ from Kipp & Zonen is given below.

- **Dust IQ:** The Dutch company, based in Delft, the Netherlands developed a product that can precisely measure transmission loss and soiling ratio known as DustIQ. The device consists of mini PV module, two Dust IQ sensors and Junction box. The device is framed with an anodized aluminum, with glass as front cover. The PV module has ethylene-vinylacetate (EVA) in between front and back side both [16]. The Dust IQ is shown in figure below:

Figure 1.5: Dust IQ with sensors on.

The device measures light scattered light from internal LED due to the the soiling on top of the glass panel. It uses optical soiling technology measurement (OSM), shown in fig 1.6 [16]

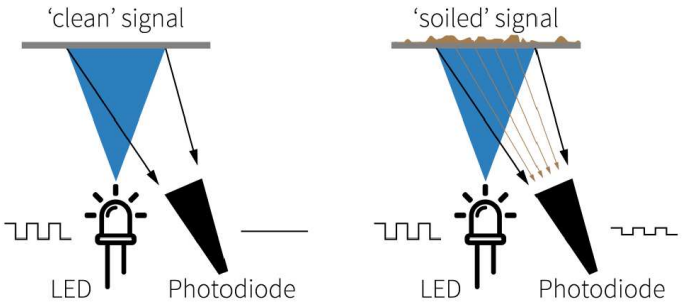

Figure 1.6: Dust IQ working principle [16].

The two OSM sensors determines the transmission loss and also the soiling ratio(SR) using the automatic calculations. The device is factory calibrated using standard Arizona test dust to perform the transmission loss calculations but the dust color and sizes varies with location. Therefore, using the on-board mini Poly crystalline silicon PV module it is possible to calibrate the Dust IQ on site for specific location with few minutes [16].

Figure 1.7: Dust IQ in the field.

1.2.5. Shading losses

The PV market is growing exponentially recently and one of major issue for PV installation is to find out a optimal location for its installation. The shading losses should be considered before installing PV systems in certain locations since, the power output of PV systems decreases drastically due to shading. The shading caused by moving clouds or various atmospheric conditions is known as dymanic shading which causes irradiance level to fluctuate within a short time interval. The shading caused by physical objects such as trees, building shadows, dust particles, snows are known as static shading which is constant for certain period of time.

The shading which is due to patches accumulating of certain foreign objects, or certain area of PV module under the shadow of other object is known as partial shading [17]. The shading in which the soil or dust is deposited uniformly over PV module is known as uniform shading. The shading drastically decreases the performance of PV module because the efficiency of PV module will decrease. Due to continuous shading the panel also degrades at faster rate leading to faster ageing of PV module [18].

(a) shading due to buildings [19]

(b) Snow [20]

Figure 1.8: Partial shading caused by various sources.

The solution to overcome shading problem can be done by integrating Bypass diode in the PV module. The bypass diode also prevents from localized overheating of the shaded cell. The working principle of PV module is shown in figure below.

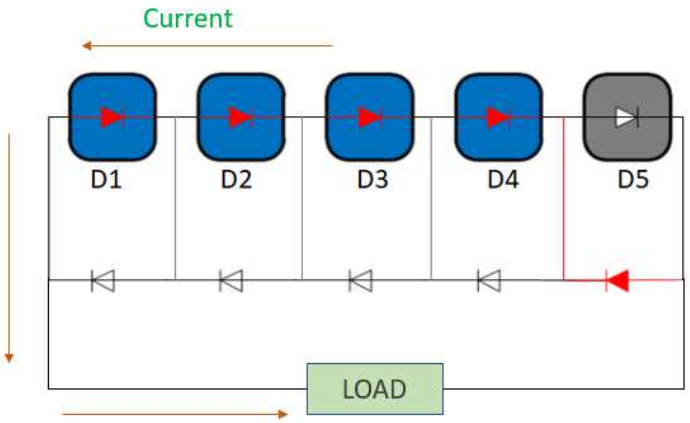

Figure 1.9: Working principle of Bypass diode

As shown in the figure 1.9, which has five PV cells in series connection where the fifth cell is shaded. The current is passed by the Bypass diode which is connected in parallel with the cell [10]. The current is no longer affected by the shaded cell preventing dissipation of energy and potential breakage of cell due to overheating. The bypass diose remains neutral when cells are not shaded [10].

1.3. Thesis motivation and research questions

The immense installation of PV systems globally is influenced by various factors as discussed in previous sections which decreases the optimal output. rradiance sensors are nowadays an integral part of the PV world since they measure the incident POA irradiance which forms a crucial part in the calculation of the performance ratio of the system and help study its performance. There are various types of irradiance sensors available in the market with slightly different performance. The accuracy of this kind of sensors depends upon the design and calibration procedure.
Kipp & Zonen a company based in Delft, The Netherlands developed a sensor known as DustIQ which predicts the soiling in PV panels. DustIQ has a mini PV module which is used for calibrating the soiling sensing sensors. The purpose of this thesis is to make the DustIQ multi-functional by converting it into PV irradiance sensors. While investigating the calibration procedure for DustIQ PV module necessity for the development of Primary reference cell was felt. The primary reference cell is developed following the ASTM 1362 calibration standard.
In this thesis, the performance of different irradiance sensors available in the market is evaluated. The various cost-effective sensors data such as Silicon pyranometer, silicon sensor are evaluated based on CMP21 pyranometer data which is regarded as the most accurate sensor. This was conducted to

1. **What is the procedure to develop a primary reference cell?**

   The details about the Primary reference cell development is discussed in chapter 2.

2. **Can Dust IQ PV module become a reference cell? If so, by which design or method?**

   Chapter 4 gives answer about the possibility of developing Dust IQ PV module as Primary Reference cell.

3. **How are the cost-effective sensors performing when compared with pyranometer?**

   The cost effective sensors performance is validated in chapter 5.

4. **How accurate is the DustIQ data in contrast to other PV reference cell?**

   The uncalibrated Dust IQ PV module performance with respect to calibrated Reference cell is presented in chapter 4.

1.4. Thesis outline

This thesis consists of 6 chapters. The research questions will be answered in these chapters. The brief description of each chapter can be found below:

Chapter 2 - Design of Reference cell In this chapter, the mechanical structure of the reference cell and different instruments involved during the experiments is presented.

Chapter 3 - PV cell characterization This chapters provides details about the PV cells used in Primary reference cell. The characterization procedure of PV cells and results obtained are also discussed.

Chapter 4- Calibration of PV reference cell Here, the calibration procedure of Primary reference and DustIQ mini PV module is presented. The results obtained after the calibration is also discussed in this chapter.

Chapter 5 - Data analysis: In this chapter, the variation between the output between cost-effective sensors and Pyranometer is evaluated. The uncalibrated DustIQ mini-PV module performance in contrast to calibrated Reference cell from is presented in this chapter.

Chapter 6- Conclusion and Recommendations: Results obtained for the proposed research questions is summarized. Finally, recommendations for future work are presented.

2

Design of PV reference cell

The solar industry is growing massively in global scale. The industries are investing a huge sum of money in research and development to manufacture the PV cells with better characteristics. These PV cells are compiled together to manufacture a PV module which can comply with the customer preference of obtaining the most efficient and cheapest PV module as possible. The PV systems are highly affected by the various environmental and technical factors as discussed in previous chapter. The irradiance sensor plays a significant role to check the output behaviour of the PV system. In this chapter, the design of a PV reference cell by Kipp & Zonen as a new irradiance sensor for the company will be discussed.

2.1. Physical specification of Reference cell

There are two types of reference cell primary and secondary cell described by ASTM and IEC standards. It gives specifics regarding the selection of Primary Reference but the Secondary reference is customer dependent [21]. If any of the major specifications from the standards are missing the reference cell is regarded as working class reference cell. The physical specifications for Primary and secondary reference are given below:

1: Primary Reference cell The Primary reference cell is calibrated in the outdoor environment directly under sunlight following test method ASTM E1125 or IEC 60904-4 [22][23].
The PV cells size in the primary reference cell should be 20 $\times$20mm^2 [22]. The mechanical housing should have a field of view of greater than 160°for the PV cell. The design should have low thermal mass with small and durable packaging which should match world photovoltaic scale(WPVS) reference cell design. The WPVS design gives preference to Mono C-Si due to its quality and stability [24]. The changes in PV cells can be considered according the industry preference. The window should be fused silica for a primary reference cell with surface thickness of 40nm/mm [21]. The temperature sensor should be standard pt100, with good internal wiring and connectors.The packaging design will be discussed later in section 3.2.

2: Secondary Reference cell The cell can be calibrated both indoor and outdoor environments against the primary reference cell following the test method ASTM 1362 or IEC 60904-2 [23][25].
The physical dimensions of the housing and PV cells size are not specified for secondary reference cell so, it depends upon the customer preference. The PV cell to be calibrated should resemble the characteristics of PV module thermally and optically. The temperature sensor should standard class A pt100, with reliable internal wiring and compatible connectors. In this study, the mini PV module in Dust IQ calibration procedure to make it a Secondary reference cell or a multi- cell reference device. The design of mini PV module is discussed in section 3.2.

2.2. Design of Reference cell

In this section, the components required within a reference cell, and a mechanical design of Primary reference cell is discussed.

2.2.1. Components required within a Primary reference cell

The reference cell requires different components integrated within it to be considered as PV reference cell. These components are discussed below:

1: Temperature sensors The ASTM standards mention that temperature sensor should be class A Pt100 sensor which should be according to DIN EN 60751 standards. The 2 pin Pt100 class A (RTD) being used in the PV reference cell is from Thermo- Electro B.V. located in the Netherlands. The resistance temperature detectors (RTDs) is made by winding a platinum wire onto the glass core and then fusing the exterior with glass. The HG1310 2 PIN RTD is suitable for a wide range of temperature (-200°C to 450°C) and corresponds to DIN EN 60751 [26].

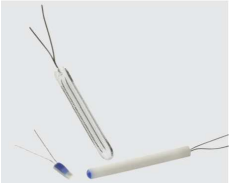

Figure 2.1: Temperature senor [26]

2: Connectors and cables The connectors from binder are used in PV reference cell due to its high tolerance and reliability. The connector has 8 wire connection with low impedance. The cables can withstand extreme temperatures and years of ultra-Violet (UV) exposure [27]. The yellow cable of the connector makes it distinguishable from other cables [27].

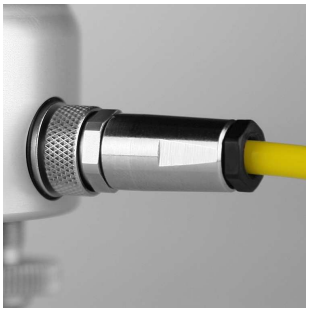

Figure 2.2: Connector and cables [27]

3: Shunt Resistor The shunt resistor required in the PV reference cell is 0.04 Ω SWD chip resistor. The resistor is connected with the wires from the PV cell to measure the short circuit current of the PV cell. The resistor is from TT electronics, a company based in the Netherlands. The resistor is very precise and stable during temperature fluctuations. To make the PV reference cell voltage reading similar to the pyranometer reading the small resistor is selected. This also makes the voltage reading from PV reference cell compatible with CR1000X datalogger.

4: Glass The standard Fused Silica glass with dimension $50 \times 50 mm^2$ is used as a cover of reference cell. The glass is exceptionally pure with transmission range from 180 nm to 2000nm, and can withstand high temperatures. The glass is manufactured by UQG Optics,England [28].

Figure 2.3: Fused silica glass [28]

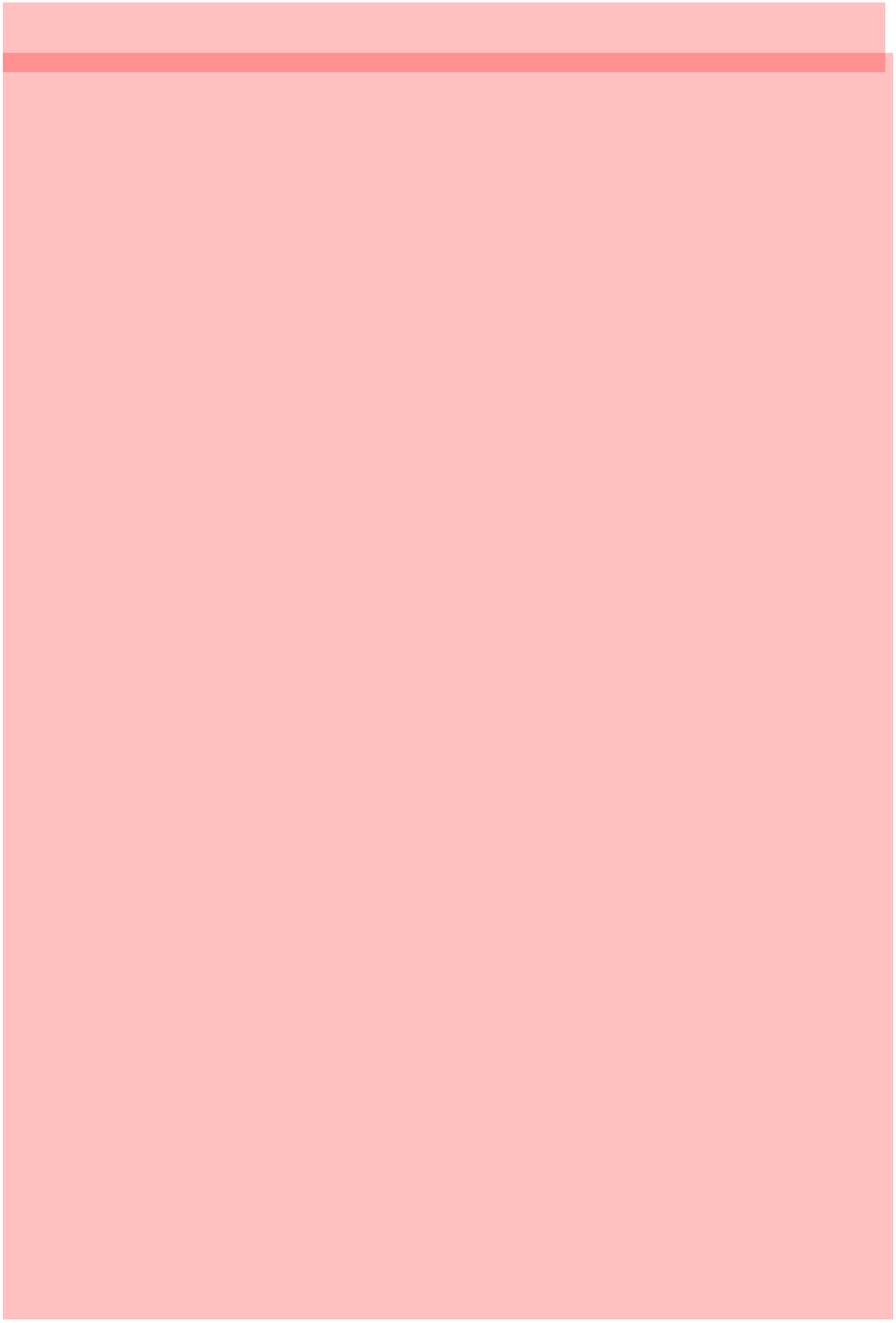

The Primary reference cell from Kipp & Zonen in real life looks like figure 2.8

Figure 2.8: Primary Reference cell

The detailed figures of mechanical housing of the PV reference cell are available in appendix-A.

3

Characterization of PV cells

The PV cell is a pivotal part of the PV reference cell. The ASTM, IEC standards provide a standard size of PV cells, and characterization to be done to consider the cell as a Primary reference cell [21]. The guidelines for Secondary and Working class differs from the Primary reference PV cell requirement guidelines. The PV cell should be exactly 20 ×20 mm^2 to be considered as the primary reference cell. The user or customer are free to choose the size of cells for secondary or working class reference cell. The type of cells is also left upon for the user to decide.

3.1. Types of PV cells

There are various types of PV cells available in the market. These cells are made up of different materials, and structures with varying characteristics. Crystalline silicon cell is the most preferred PV material as the market exemplifies. The high-efficiency C-Si is used as a PV cell in the Kipp & Zonen PV reference cell.

a.Mono C-Si Cell: The Mono Crystalline silicon PV cells are the purest form of Silicon, which has continuous lattice structure with no grain boundaries. The cells are generally manufactured by Czochralski process in which the crystals are grown to form a uniform single crystal of Silicon. The Mono C-Si PV cell which is used as PV reference cell were manufactured by Shenzhen Meisongmao Industrial Co., Ltd from Shenzhen, China one of the largest solar cells and modules distributor in China. The standard PV cell was later sliced into 20×20 mm^2 mini PV cell. The characteristics of the standard Mono C-Si cell are given in Table 3.1.

b.Poly C-Si Cell: The Poly Crystalline silicon PV cell is high purity silicon but has several grain boundaries making it easily distinguishable to Mono C-Si. It is a perfect rectangle with no round edges. Poly C-Si PV cells are generally produced by the Siemens process where the volatile silicon are separated, and small crystals are decomposed together to form a Poly C-Si. The Poly C-Si PV cell which is used as PV reference cell were developed by Chinaland solar another prominent manufacturer of solar cells and modules distributor in China. The characteristics of the standard Poly C-Si cell from the manufacturers datasheet are presented in Table 3.1.

Table 3.1: Charateristics of PV cell

	PV cells	
Parameters	**Mono C-Si**	**Poly C-Si**
Size (mm^2)	156.75 × 156.75	156.75 × 156.75
Efficiency (%)	19.8	18
P_{max} (W)	4.87	4.33
V_{oc} (V)	0.541	0.63
I_{oc} (A)	9.0	8.620
FF (%)	79.93	79.6

3.2. Characterization of PV cells

The ASTM standard mentions that the cell size should be $20 \times 20\ mm^2$ to be considered as a primary reference cell. The standard $156.75 \times 156.75\ mm^2$ PV cells was cut into $20 \times 20\ mm^2$ PV cells in the TU Delft laboratory cells by using Lasergraaf machine. The characterization was carried out for optimized Mono and Poly crystalline silicon using Wacom WXS-156S solar simulator and EQE testing set-up. The Wacom is class AAA solar simulator with temperature control block to obtain precise characterization results [31]. The Hydrogen and Xenon lamps are combined in the Wacom solar simulator has high accuracy with respect to spectral content (set of the light source), Uniform intensity (spatially uniform intensity), temporal instability (stable light source) [31]. The Wacom is shown in the figure below.

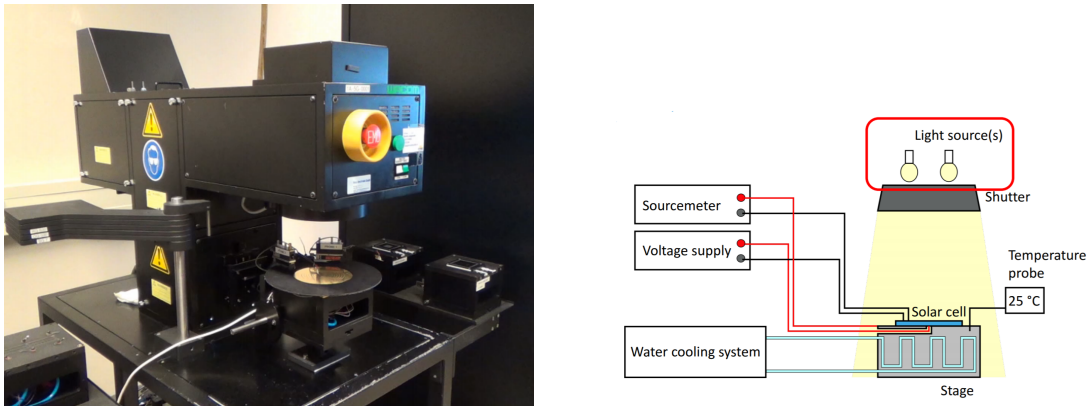

(a)Wacom at TU Delft.

(b)Wacom with solar simulator.

Figure 3.1: Solar Simulator [31]

3.2.1. Fill Factor of reference cell

The I-V curve of the cells was obtained at standard test condition(STC) using Wacom. The IV curve was generated using Wacom and software ("Wacom IV sweep $v2_{02}$") [31]. The solar simulator was left for 30 minutes to gain stability. The table shows the characteristics of optimized PV cells at STC.

Table 3.2: Characteristics of optimized PV cell

	PV cells	
Parameters	**Mono C-Si**	**Poly C-Si**
Size	20×20 mm^2	20 ×20 mm^2
Efficiency	18.5 %	16 %
P_{max}	0.073 W	0.0645 W
V_{mpp}	0.52 V	0.5 V
I_{mpp}	142 mA	129 mA
V_{oc}	0.63 V	0.61 V
I_{sc}	152 mA	138 mA
FF	77.5 %	75 %

The "fill factor (FF)" is defined as the ratio of the maximum power from the solar cell to the product of Voc and Isc. FF determines the maximum power the solar cell can produce. FF is expressed by the following equation [10].

$$FF = \frac{I_{mpp} \times V_{mpp}}{I_{sc} \times V_{oc}} = \frac{P_{mpp}}{I_{sc} \times V_{oc}} \tag{3.1}$$

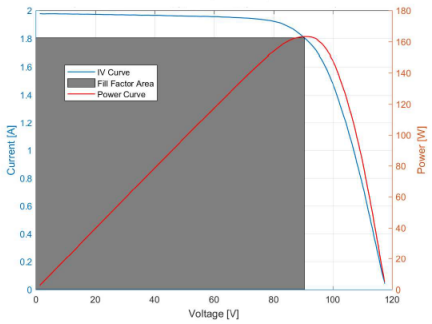

Figure 3.2: IV characteristics of PV module [9].

The "Fill Factor" measures the squareness of IV curve of the PV cells, as shown in the figure above. The solar cell with larger voltage will have higher Fill Factor. The current for both optimized Poly and Mono C-Si have decreased due to the reduction of the active surface, but the voltage only varies slightly. The influences on current lead to a lessening of Fill factor of optimized PV cells with respect to standard PV cells as seen in Table 3.2. However, the PV cells still have good "Fill factor" to be used as a standard cell for Primary Reference cell.

3.2.2. Temperature sensitivity of PV cell

The IV curve of PV cells was measured to determine external parameters for different temperature. The IV curve for varying temperature was generated using Wacom with the help water cooling system integrated into the instrument. The temperature was varied with "Wacom IV sweep $v2_{02}$" software. The effect of temperature on the IV curve and measured parameters are presented below.

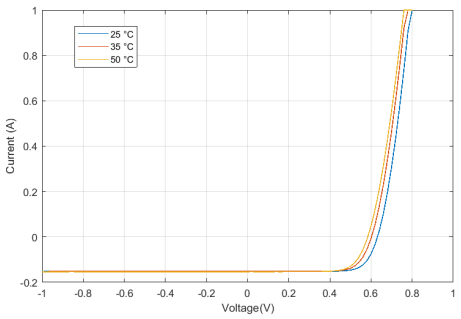

(a)Mono C-Si.

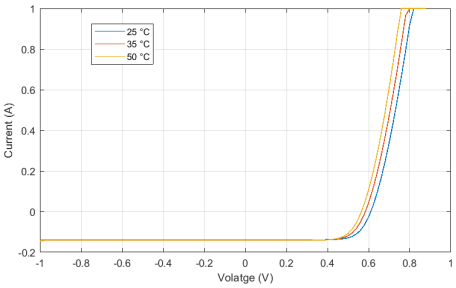

(b) Poly C-Si .

Figure 3.3: Temperature sensitivity of PV cells

From the above figures, it can be conferred that the V_{OC} of both PV cells decreased with temperature. Meanwhile, there is only a minor variation in the I_{SC}. To have a distinct picture, the V_{OC}, I_{SC}, and P_{max} of the two PV cells at different temperatures are listed in the table below.

Table 3.3: Characteristics under varying temperatures

	Mono C-Si			Poly C-Si		
Prameters	**25°**	**35°**	**50 °**	**25°**	**35°**	**50 °**
V_{oc} (V)	0.63	0.60	0.58	0.61	0.58	0.56
I_{sc} (mA)	152	152.12	153	138	141	142
P_{mpp} (W)	0.0 73 W	0.065 W	0.062	0.0645	0.0576	0.055

From the above tables, it can be seen that the V_{OC} and P_{max} for both cells decreased with temperature. Meanwhile, there is a small increase in I_{SC} of the cell. The temperature coefficients for external parameters helps to understand the influence of temperature on PV cells. The Temperature coefficients for PV cells can

be obtained by using the following equation [10]:

$$\alpha_{V_{OC}} = \frac{V_{OC,T} - V_{OC,STC}}{V_{OC,STC} \times (T-25)} \tag{3.2}$$

$$\alpha_{I_{SC}} = \frac{I_{SC,T} - I_{SC,STC}}{I_{SC,STC} \times (T-25)} \tag{3.3}$$

$$\alpha_{P_{MPP}} = \frac{P_{MPP,T} - P_{MPP,STC}}{P_{MPP,STC} \times (T-25)} \tag{3.4}$$

where,

$\alpha_{V_{OC}}$, $\alpha_{I_{SC}}$ and $\alpha_{P_{MPP}}$ are temperature coefficients for voltage, current and Maximum power points

$V_{OC,T}$, $I_{SC,T}$ and $P_{MPP,T}$ are voltage, current and Power at varying temperature

$V_{OC,STC}$, $I_{SC,STC}$ and $P_{MPP,STC}$ are voltage, current and Power at Standard test condition

The temperature coeffecients for respective PV cells are presented in Table 3.4.

Table 3.4: Characteristics under varying temperatures

Parameters	Mono C-Si [%/ °C]	Poly C-Si [%/ °C]
$\alpha_{V_{OC}}$	-0.32	-0.33
$\alpha_{I_{SC}}$	0.026	0.11
$\alpha_{P_{MPP}}$	-0.6	-0.36

As seen in the above table, PV cells are immensely influenced by temperature. The V_{OC} and P_{max} are negative since it decreases with temperature. The open circuit voltage V_{OC} is the most influenced parameter, and short circuit current I_{SC} increases with temperature. The bandgap of a semiconductor decreases with increasing temperature, and more photon is absorbed resulting in more photogeneration. This leads to slight increment in short circuit current, I_{SC}, which is negligible. However, reduction in bandgap also leads to heavy decrements in open circuit voltage effecting the PV cells overall performance. This is illustrated by the following equation [10].

$$V_{OC} = \frac{kT}{q} \ln\left(\frac{J_{SC}}{J_0}\right) \tag{3.5}$$

3.2.3. Linearity of short circuit current of the cell with respect to irradiance

Here, the performance of the PV cell based on varying irradiance were analyzed. The lenses with distinct optical density were placed above the solar cell to vary the light intensity. Figure 3.4 shows that only part of the light is transmitted, the rest of them either absorbed by glass or reflected back.

Figure 3.4: UV reflective OD filters

The lenses are available in various optical density(OD), the irradiance value for each optical density can be obtained using following equation [31].

$$OD = -log_{10}\left(\frac{G}{G_{STC}}\right) \tag{3.6}$$

Where, G_{STC} is irradiance at standard test condition, and G is irradiance obtained after light passes through filter. The short circuit current, I_{SC}, obtained for the different irradiance is tabulated in table 3.5. It shows that short circuit current of PV cells is directly proportional to irradiance,

$$I_{SC} = \beta G \tag{3.7}$$

Here, β is proportionality constant.

Table 3.5: Short circuit current based on changing light intensity.

		Mono C-Si	**Poly C-Si**
OD	Irradiance (W/m^2)	I_{SC} (A)	I_{SC} (A)
0	1000	0.152	0.139
0.1	794.33	0.112	0.103
0.5	316.23	0.038	0.037
0.6	251	0.031	0.029
1	100	0.013	0.012
2	10	0.004	0.004

The figure 3.5 shows the linearity of short circuit current with respect to varying light intensity. The short circuit current decreases linearly as the irradiance decreases.

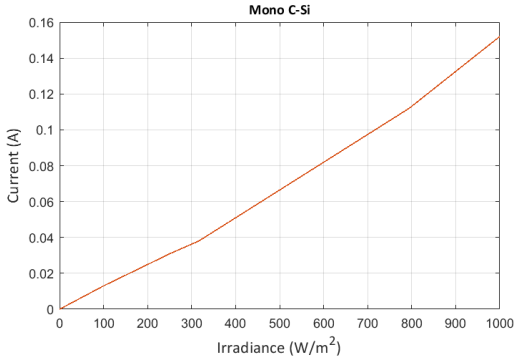

(a)Mono C-Si.

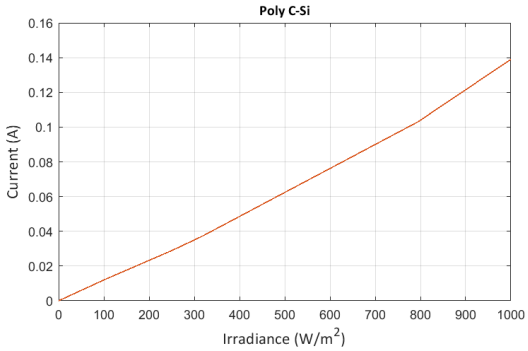

(b) Poly C-Si .

Figure 3.5: Linearity of short circuit current vs irradiance

The linearity check performed is not accurate due to uncertainties in the solar simulator and lenses. Therefore, the non- linearity is calculated to make corrections in linearity measurements. The equation to estimate non-linearity(∇_{NL}) is [32]

$$\nabla_{NL} = \left(\frac{P_{STC} \times I}{I_{STC} \times P}\right) - 1 \tag{3.8}$$

Where, P is the power incident on device under test, and I is the current of device under test. The following graph shows shows the non-linearity between short circuit current of cell with respect to varying irradiance.

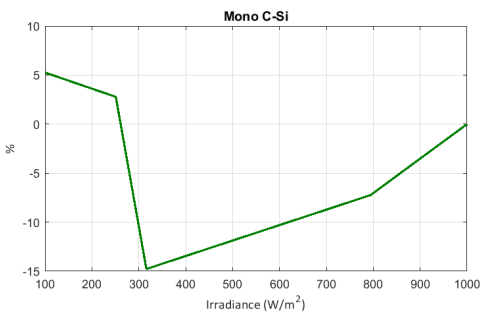

(a)Mono C-Si.

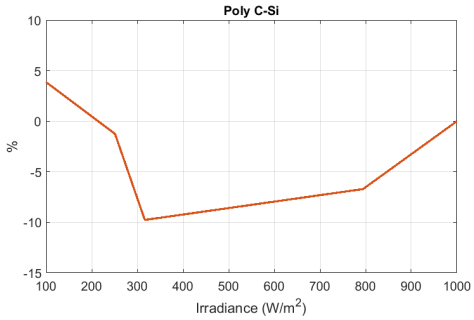

(b) Poly C-Si .

Figure 3.6: Non-Linearity of short circuit current vs irradiance

3.2.4. External Quantum Efficiency of PV cell

The External quantum efficiency(EQE) is the number of electron- hole pair generated to the incident photon per unit time. The EQE of the cell is defined as [31];

$$EQE = \frac{I_{ph}(\lambda)}{q \times \phi(\lambda)} \tag{3.9}$$

where $\phi(\lambda)$is the spectral photon flux incident on the PV cells, q is the elementary charge and I_{ph} is the photocurrent generated. The EQE is measured by illuminating the solar cells by monochromatic light and I_{ph} is measured through the solar cells at different wavelength (λ). This shows that the EQE is wavelength dependent.

The EQE measurement set up consists of a light source as a Xenon lamp, chopper frequency generator, the monochromator, a lens system, and Lock-in amplifier. The light from Xenon lamb, which has even spectral distribution passes through a filter to prevent interference of short wavelength with a long wavelength. Then the light is chopped by chopper wheel to get the on-off frequency of 123 Hertz. The monochromator selects a narrow band of wavelengths from the incoming chopped light. The monochromatic light is focused on solar cells through the lens system. The solar cell under test produces a current which passes through shunt resistance, and the voltage drop is measured. The lock-in amplifier is used to filter the solar cell's response to monochromatic light from noise by comparing with light at the chopper [31].

The figure 3.7 shows the EQE measurement set up at TU Delft laboratory. The set up consists of all the required objects as mentioned before for EQE measurement. The wavelength range and step size can be defined in software "MAIN QEM 3.0"[31]. The calibrated silicon reference diode is used for calibration to measure the photon flux precisely for each wavelength before measuring the sample PV cell. After calibrating the entire set up the PV cell was placed on the mounting frame. The contact probes are connected on the front contact and back contact of PV cells. The light spot should be placed in such a way to avoid shading due to fingers. The EQE curve for PV cells can be seen in the "MAIN QEM 3.0" software for the specified wavelength range.

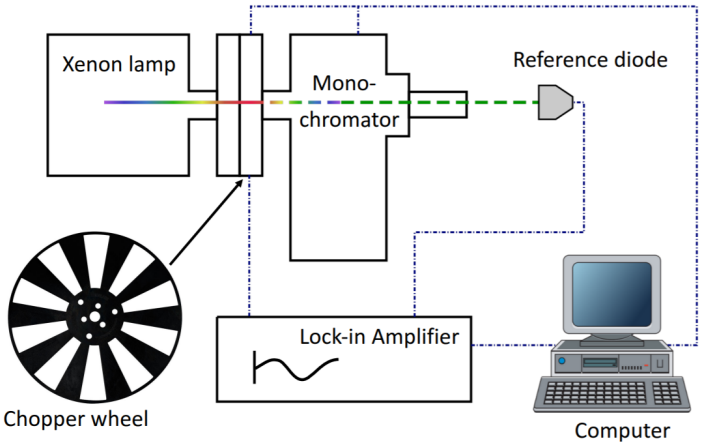

Figure 3.7: External Quantum Efficiency set-up (TU Delft lab) [31]

The EQE for Mono and Poly Crystalline silicon cell obtained as seen in figure below. The wavelength range was specified from 300 nm to 1200 nm which the response range of typical C-Si cell.

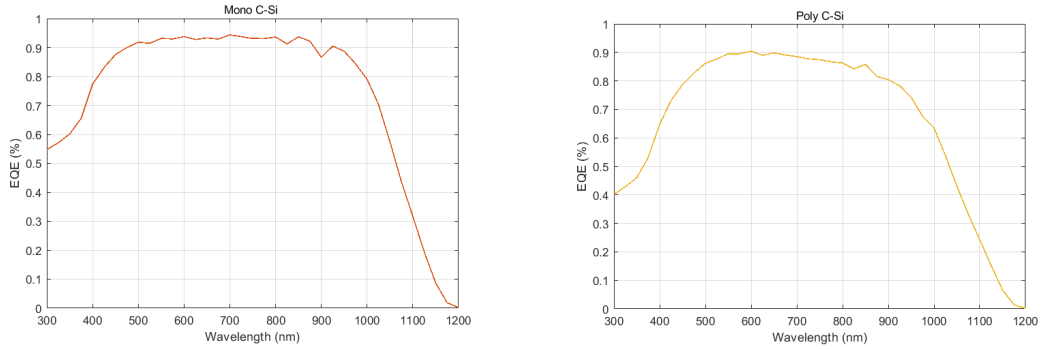

(a)EQE of Mono C-Si PV cell. (b)EQE of Poly C-Si PV cell.

Figure 3.8: External Quantum Efficiency (EQE)

The EQE of the Mono C-Si cell and Poly C-Si is around 95% and 90% in the mid wavelength ranges. It also demonstrates that EQE is higher for Mono C-Si than Poly C-si. The EQE measurement is influenced slighly by the distance between the fingers of respective cell. The EQE of overall PV reference cell including the fused silica glass is shown in figure below.

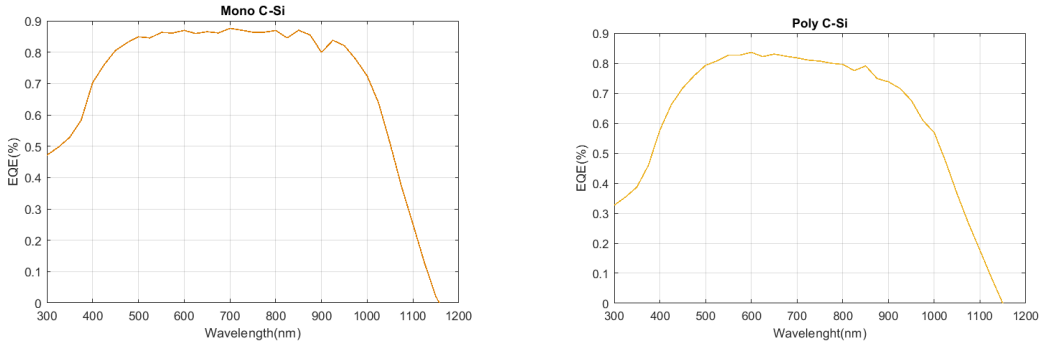

(a)EQE of Mono C-Si PV cell. (b)EQE of Poly C-Si PV cell.

Figure 3.9: External Quantum Efficiency (EQE) with fused silica glass

3.3. Uncertainties and experimental error

The devices used for the measurements has seen some degradation over time due to prolonged uses. The solar simulator Wacom consists of two light source Halogen and Xenon lamp, where the halogen lamp is prone to wearing out if used for a long time. Xenon lamp efficiency also decreases over time. The lenses used during the linearity measurement had some scratches and dirt on it leading to marginal uncertainties. During the linearity measurement, the reflected light sources from the surrounding were incident on the PV cells causing deviation from actual measurement values.

The EQE set-up consists of a Xenon lamp, which efficiency decreases gradually due to continuous usage. The light from the Xenon lamp travels through different instruments leading to fluctuations in light intensity before reaching the device under test. The EQE measurement device at TU Delft was specially designed for Amorphous silicon cell, the cell with a wider gap between the fingers. The device under test for our case was crystalline silicon cell with a small gap between the fingers. The narrow beam of the light source was slightly over the fingers causing shading, which leads to a certain error during the EQE measurements. The EQE measurements are not completely isolated from the external light source. The parasitic external light source and uncertainties in various devices used during the measurement immensely impact the EQE measurements. The opening where the signal generators are kept leads to parasitic light source inside measurement set-up

In the next chapter, calibration techniques of Primary Reference cell is discussed. The techniques are then applied to calibrate the Primary reference cell in Delft, The Netherlands and Almeria, Spain.

4

Calibration of Reference cell

It is important to know the performance of the installed PV systems. The calibrated PV reference cell plays a vital role to determine the performance ratio of PV systems. The standards such as ASTM, IEC has precise calibration procedures, which are accepted worldwide. Taking into account the time, conditions, instruments, calibration procedure, and the structure of the device to be calibrated, the reference cell is divided into different classes.
In this chapter, we first look into the calibration procedure of Primary reference cell and calibration value of the reference cell is calculated. Next, the procedure applicable to develop Mini- Module in DustIQ as a reference device is investigated.

4.1. Calibration of Primary Reference cell

"Calibration" is the methodology to compare the results of the device under test with the standard values to verify the new product gives precise results. The Primary reference cell is the PV cell calibrated against direct sunlight,traceable against the SI units. The device should have small package design as discussed in chapter 2, which should have a field of view of 165° and low thermal mass. The crystalline silicon cell is preferred with a standard dimensions $4cm^2$. The PV cell should be characterized before calibrating following the procedure mentioned in chapter 3. The various instruments used for calibrating the reference cell are described elow.

a) Absolute cavity radiometer:

The PMO6-cc from Davos Instruments, is an absolute cavity radiometer calibrated according World Meteorological organization(WMO) standards. The instrument measures direct solar irradiance(DNI). The instrument has two cavities a reference cavity and an active cavities [33]. The difference of radiant power decreased when exposed to sunlight, gives the DNI data. The device can be used in any environmental conditions. The instrument can be controlled remotely via RS232 software or through the touch-screen integrated with the device [33]. The device is self calibrating due to periodic blocking of light due to shutter.

Figure 4.1: PMO6-cc Radiometer [33]

b) Pyrheliometer:

The Pyrheliometer is a radiometer used to measure the direct normal irradiance (DNI). The Pyrheliometer CHP1 used in this calibration procedure was developed by Kipp & Zonen. The device is known to be the best commercially available first class pyrheliometer. The CHP1 is calibrated against reference pyrheliometer traceable to world radiation center (WRC) in outdoor conditions at Davos, Switzerland. The pyrheliometer has field of view (FOV) of 5°, the slope of 1° [34]. The device gives accurate measurements when the sun is right above its head, and placed in sun tracker at certain tracking angle.

Figure 4.2: CHP1 Pyrheliometer [34]

c) Spectroradiometer:

The spectroradiometer is used to measure the spectral irradiance."Spectral Irradiance" is the irradiance as a function of Wavelength,with unit in W/m^2nm^1 [25]. Thus, it refers power incident per unit area per wavelength. The spectroradiometer "USB4000-XR1-ES" is the product from ocean optics which is used during the calibration period. The USB2000 Spectromter has a good response from 200-1100 nm which perfectly aligns with C-Si spectral response range [35].

Figure 4.3: USB 2000 Spectrometer [35]

d) Dual axis Sun tracker:

The dual axis tracker is most important device in-order to calibrate the reference cell. The 2AP tracker which is a reliable for all weather conditions and steady is used to mount the instruments to calibrate the reference cell [36]. The 2AP tracker is from Kipp & Zonen.

Figure 4.4: 2AP Tracker [36]

The instruments mentioned above were mounted on 2AP sun tracker along with the Reference cell, cooling unit and collimator tube. The design principle of cooling units and collimator tube are described in chapter 2. The data during the calibration was recorded using the Campbell Scientific CR1000X datalogger, and stored in the PC storage unit.

fi

4
F
r
d
t

4.3. Investigation of process applicable for calibrating mini- PV module in DUSTIQ

The Dust IQ consists of Mini PV module of dimensions $23.5 \times 7.7\ cm^2$ integrated in it. The working principle of DustIQ is explained in section 1.2 of chapter 1. The Mini PV Module if calibrated will be considered as large scale reference cell. Here,the procedure which can be used in the future to calibrate the DustIQ PV cell will be discussed.

Figure 4.7: Mini PV module in Dust IQ.

The outdoor calibrations of reference cell require a collimator tube which should match the field of view of pyrheliometer. The Mini PV module dimensions are way big to design the specified collimator tube so, it is not possible to calibrate the DustIQ mini PV module outdoor. The PV module can be calibrated indoor using the class AAA solar simulator. The class AAA solar simulator has high accuracy with respect to spectral content (set of the light source), Uniform intensity (spatially uniform intensity), temporal instability (stable light source) [31]. The 19 different LED'S are used to develop class AAA nowadays. Hydrogen and Xenon combined together it can also be used as class AAA solar simulator [31]. The solar simulators can be built in the Kipp & Zonen product development unit or can be brought from different suppliers around the globe.
Some of the prominent manufacturers of class AAA solar simulator suitable for DustIQ are listed in the table below:

Table 4.1: Statistical Parameters

Company	Model	Beam size	Price (USD)
Newport	Oriel Sol3A	$30.5 \times 30.5\ cm$	$16000 approx
Photonicssolutions	UHE-33	$33 \times 33\ cm$	$68000 approx
Photonicssolutions	UHE-45	$45 \times 45\ cm$	$68000 approx
Eternal sun	LASS	-	-
Reoo	GTM-3B	$200 \times 110\ cm$	$9000 approx
OAI	TriSOL	$30 \times 30\ cm$	$49000 approx

The characterization of the mini PV module will be the same as the Primary reference cell calibration procedure. The omission of a few characterizations mentioned will lead to a reduction in a class of Reference

After the calibration procedure, the calibration factor should be calculated. The calibration value must be calculated for respective data points by using the equation 4.9 [25],

$$C = I_D \times \frac{C_R}{I_R \times M_i} \tag{4.9}$$

Where C_R is calibration value of source devic, and M_i is spectral mismatch parameter. If the transfer calibration method was followed use the succeeding equation to get calibration value for each data point [25],

$$C = I_D \times \frac{C_R}{C_T \times I_R \times M_i} \tag{4.10}$$

Finally, the average of all the calibration value is computed to get a single calibration factor.

4.3.1. Dust IQ Calibration Test in TU Delft

The Dust IQ has a Mini PV module which requires a large class AAA solar simulator in order to be calibrated. A test was conducted at TU Delft laboratory in the large class AAA solar simulator from the eternal sun known as LASS [37]. The solar simulator from the eternal sun temperature rises quickly within a few minutes which is not suitable for calibration. The temperature racked up to almost 70°C during the test period. The solar simulator temporal stability is also high which requires the monitor to transfer the calibration. The Kipp & Zonen can work on the suitable cooling system for Mini PV module in Dust IQ to make the calibration in eternal sun solar simulator possible. An alternative method can be changing the wiring configuration of DustIQ mini PV module. Out of six PV cells in DustIQ connecting only one cell electrically will make the calibration and characterization procedure easier.

Figure 4.10: Solar simulator- LASS [37].

In the next chapter, the data analysis of various irradiance sensors located on the rooftop. The data analysis is carried out to check the variation between the different sensors data with respect to pyranometer.

5

Data Analysis

In this chapter, a brief information about the different types of solar irradiance measurement device are presented. Following a brief introduction about sensors the data processing methods are discussed. Finally, the data analysis is carried out for various instrument considering pyranometer data as a reference.

5.1. Solar irradiance measurement instruments

There are various types of solar irradiance measuring instruments available in the market. Kipp & Zonen is one of leading company manufacturing irradiance sensors such as Thermopile Pyranometer (CMP21), Silicon pyranometer, Pyrheliometer, Cavity Raidiometer and many others. In the terrace of Kipp & zonen three silicon Pyranometer and one silicon sensor from are installed which are recognized as cost effective sensors. The irradiance data from cost effective sensors is compared with the data from thermopile pyranometer installed right beside these cost effective sensors. All sensors are in same plane of array (POA) with repsect to Poly C-Si PV panel from Canadian solar. The figure 5.1 shows the different devices installed at the roof of Kipp & Zonen.

Figure 5.1: Instruments at Roof of Kipp & Zonen .

The description of the irradiance sensors installed in the roof is given in Chapter 1. The tilt angle of all the sensors positioned is 30°.

5.2. Data processing

The various irradiance senors,temperature data from the rooftop installation at Kipp & Zonen were used. The Air Mass (AM) value was calculated using equation 5.3. The Air mass is selected to check variation as it has heavy influence on the performance of an irradiance sensor.
Next, the data were aggregated in a minute by minute format for the research purpose. The morning data were removed from the datasets due to huge constant shading of instruments. The shading was due to trees, chimneys, and buildings surrounding the places where the instruments were located. The missing gaps and outliers between the data were removed using a simple code in Matlab. The equations used to remove the

outliers are as follow:

$$UB = Q3 + 1.5 \times IQR \tag{5.1}$$

$$LB = Q1 - 1.5 \times IQR \tag{5.2}$$

Here, Q3 and Q1 are third and first quartile respectively. UB and LB are upper and lower bound respectively and IQR is inter-quartile range.The data which were lower than LB and greater than UB were removed. The PV reference cell had the most outliers. The dataset for PV reference cell reduced after the outliers were removed.

5.2.1. Data Analysis method

The reference instrument is taken as CMP21 Pyranometer. The differences between the reference instrument and test instruments are evaluated to know the performance of test instruments. The test instruments are cost-effective sensors including DustIQ. The difference between the data of reference and test is considered as an "error". If the median of the distribution is not equal to pyranometer value there is a bias in the test instruments. Further assessment was carried out with the help of statistical indicators such as bias,mean absolute error (MAE) and root mean square error (RMSE). The equations for the statistical indicators can be written as [38],

$$MAE = \frac{\sum_{i=1}^{n} |M_i - C_i|}{n} \tag{5.3}$$

$$RMSE = \sqrt{\frac{\sum_{i=1}^{n} (M_i - C_i)^2}{n}} \tag{5.4}$$

Where, M_i is the data from Pyranometer and C_i is data from cost effective sensor. The MAE is the average absolute difference between reference and test device. The RMSE helps to determine how close the reference and test datasets are. The RMSE will be high if there is an enormous difference between reference and test data. The boxplot diagram is used to represent the quantiles of the errors. The boxplot will help to get an inclusive view of error distributions. The data sets are further divided into subsets for winter and summer weather to determine the performance of the instruments during those conditions.

5.2.2. General performance of sensors

Figure 5.2 shows the error distribution of datasets for the sensors mentioned in section 5.1. The boxplot demonstrates the IQR range (bluebox), the median (red line), and the extended range of the data distribution without outliers. The boxplot of the relative error distribution is in Appendix B.

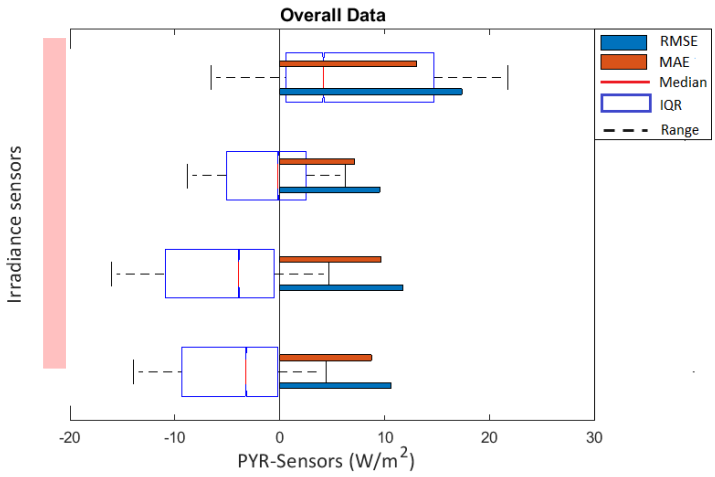

Figure 5.2: Boxplot diagram of the overall error distributions

The acronyn is for three silicon Pyranometers respectively. The acronym is for silicon sensor from Mencke & Tegtmeyer, and PYR stands for thermopile pyranometer (CMP21). The ensors deviates when compared with a thermopile pyranometer. The expended error distribution

ranges from -16 W/m^2 to 5 W/m^2 (-9% to 3%). Both underestimates the irradiance with median error bias by -5 W/m^2 (-3 %), respectively . For , the bias error is -1 W/m^2 which is significantly lower. The error range for l is -8 W/m^2 to 8 W/m^2 (-5% to 5%). Among all the sensors, the has the highest bias error and error range. The error overestimates the irradiance with error ranging from -8 W/m^2 to 22 W/m^2 (-2% to 6%) with a bias of 6 W/m^2. The relative error distribution is low for sensor due to removal of outliers.

Alongside respective boxplot, the magenta and the cyan bars show the RMSE and MAE. The statistical estimators are also high for ensor and low for sensor. The PV reference cell ( ) overestimates the irradiance during certain time interval leading to higher RMSE ,and MAE is high due to mismatch between irradiance data when compared with pyranometer. The also overestimates the irradiance output leading to RMSE. The silicon sensor has temperature correction which makes the sensor more accurate compared to two other silicon sensor

5.2.3. Performance for specific conditions

Here, the performance of irradiance sensors during summer months with high sun elevation, more sun hours and mostly sunny days, and during winter months with Low sun elevation, less sun hours and fluctuating weather conditions (Sunny, cloudy and snowy days).

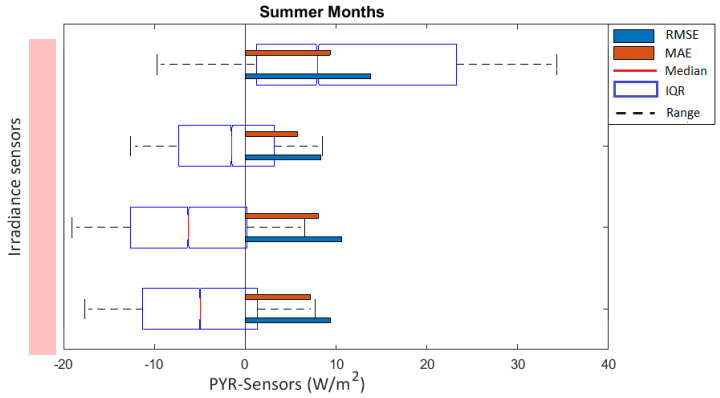

(a) Error distribution during summer

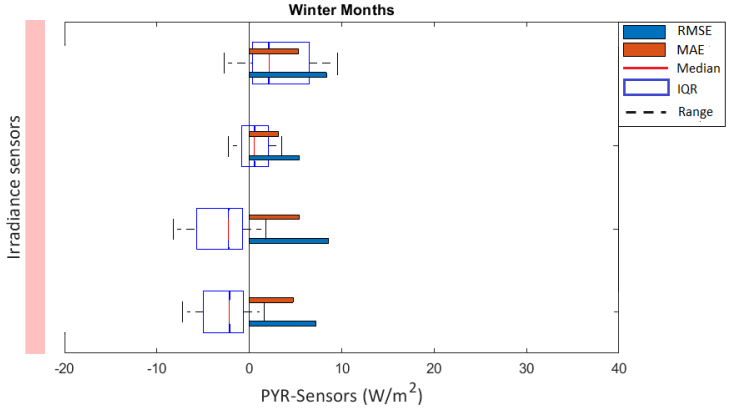

(b) Error distribution during winter

Figure 5.3: Boxplot diagrams of the error distributions at different conditions.

Figure 5.3a shows has similar error distribution. The error distribution ranges from -18 W/m^2 to 8 W/m^2 (-8% to 3%). The devices underestimates the irradiance with bias of -7 W/m^2 (4%) and -6 W/m^2 (3%) for respectively. The has expanded error distribution of -12 W/m^2 to 10 W/m^2 (-4% to 3%), and slightly underestimates the irradiance by 2 W/m^2 (1%) when compared with pyranometer. The bias error for is 8 W/m^2 (3%) and error ranges from -10 W/m^2 to 33 W/m^2 (-1% to 5%).

The relative error distribution boxplot is in Appendix B. The relative error distributions for the device

is slightly higher during winter months compared to summer months. The sensor have relative error distribution of -5% to 8% in winter months vs -4% to 3% during summer months. The error distribution has variation during two different climatic conditions for all the sensors due to the difference in sun hours, fast-moving clouds which cause shading, fluctuating temperatures, the sun is low in the sky during winter. The snow, fog, water droplets cause high variation between the data. The winter months have few data points due to fewer sun hours, which leads to higher relative error distribution compared to summer months.

5.3. Comparison of DustIQ mini-PV module with Pyranometer

DustIQ consists of six PV cells connected as a mini-PV module. The PV cells in DUSTIQ has not been calibrated according to the standard to be considered as a PV reference cell. The irradiance data from the PV module in DustIQ is compared with the Plane of array data from pyranometer. The irradiance data of DustIQ is calculated with help of parameters obtained from LASS solar simulator in TU Delft laboratory.The reference short circuit current at standard test condition is 1.1 A, and temperature coefficient for short circuit current is taken as 0.053 (%/°C).

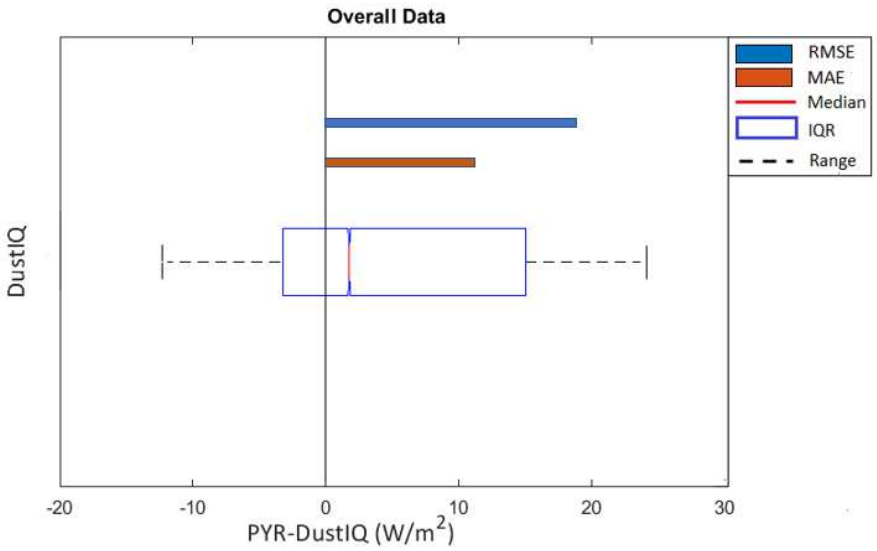

Figure 5.4: Overall error distribution of Pyranometer v/s DustIQ PV Module

Figure 5.4 shows the expanded error distribution ranges from -15 W/m^2 to 25 W/m^2 (-12% to 10%). The bias error for DustIQ PV cells is $4W/m^2$ (2%).The statistical errors RMSE and MAE is 19 W/m^2 to 13 W/m^2 respectively. The DustIQ PV module even though not calibrated according to the standards is still comparable to the output of silicon sensor from M The comparison between two PV silicon devices are shown in table below:

Table 5.1: Statistical Parameters

Error		DustIQ
MAE (W/m^2)	9	13
RMSE (W/m^2)	14	19
Bias error	6	3

The statistical error is slightly higher for DustIQ PV module compared to the silicon sensor which can be due to a large area of the Mini-PV module compared to the small area of Mencke & Tegtmeyer. The bias error of the DustIQ better considering silicon sensor bias error. Therefore, the performance of DustIQ PV module can better the working class reference cell ( ) if calibrated according to high-class standards. The investigation of the calibration procedure for the PV cells in DustIQ is presented in section 4.3 of chapter 4.

5.4. Variation between irradiance sensors due to Air mass

In this section, silicon photodiode pyranometers and silicon sensor) will be compared with Pyranometer based on varying Air mass. The silicon pyranometers and silicon sensor are currently prevalent instruments to measure the PV usable light. The sensors have a fast response rate, easy maintenance and most importantly low price are the reason behind the popularity of these sensors in the PV industry.

Air mass (AM) is the path the sunlight has to travel through to reach the earth surface. As the sunlight passes through the atmosphere it gets attenuated, due to absorption and scattering [39]. The sunlight passes through the minimum atmosphere when the sun is directly overhead, known as AM1. The path length for sunlight to travel through the atmosphere increases with increasing Air mass. The AM increases when the sun is closer to the horizon. The "AM1.5" is the standard condition universally accepted to characterize the solar cells [40]. The Air mass is calculated using the following equation [10].

$$Airmass(AM) = \frac{e^{-z/z_h}}{Sin(a_s)) + 0.5057.(a_s + 6.08)^{-1.634}} \tag{5.5}$$

where, z is the site altitude which is 10 m, z_h is the scale height of the Rayleigh atmosphere near the Earth surface which is 8434.5 m, and a_s is the sun altitude which extracted from KNMI website.
The graph below shows variation of the silicon photodiode pyranometers and silicon sensor (output with respect to Pyranometer output based on Air mass.

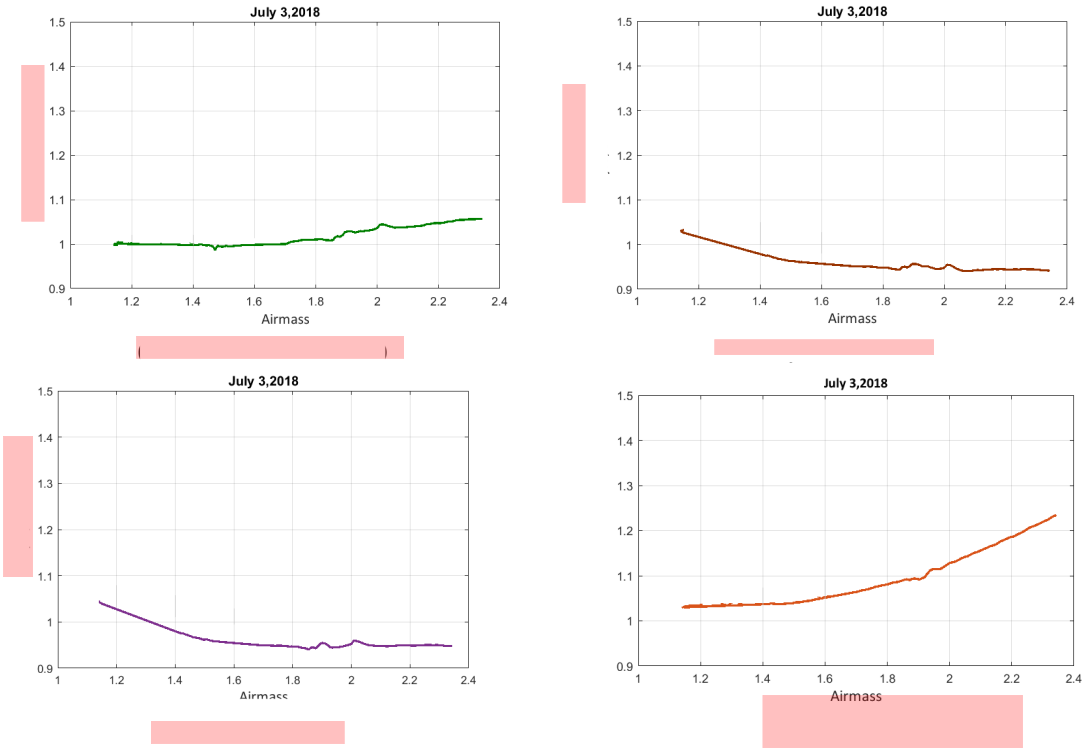

Figure 5.5: Variation of between various sensors with respect to Pyranometer based on Airmass

July 3, 2018, was observed as a clear day in Delft, The Netherlands. The data is hugely influenced by shading from buildings, trees, chimneys, and temporary blockage of sight. The huge fluctuations in the graph are due to the aforementioned problems. The perform better during higher Air mass or higher Zenith angle compared to lower Air mass which is the blue region of light. The another silicon pyranometer which agree with Pyranometer irradiance output during low Airmass and slightly underestimates during high Airmass. The response is better than s because the device is temperature corrected while are not temperature corrected. PV reference cell) slightly underestimates during low Air mass, and has a bad response during high Air mass leading to massive overestimation.

The aerosols are fine particles or gas filling the atmosphere causes the scattering of sunlight which influences the spectral distribution [41]. The pathlength for sunlight is high when it is low in the horizon, which

leads to absorption and scattering of light causing differences in spectral distribution between the irradiance sensors [41]. The high aerosols also causes scattering in the blue part of the solar spectrum causing under and over prediction when compared with well-calibrated Thermopile Pyranometer. The irradiance devices are calibrated at different zenith angle, temperature, and Air mass which makes devices to perform different during the varying atmospheric condition. The error during Air mass calculation also causes an error in the relative response of the sensors [42].

5.5. Conclusion on sensor performance

The 8 months of data collected from different cost-effective sensors were compared with Pyranometer data. The sensors were placed in the same plane of the array. The relative error distribution graph is available in appendix B.

The overall performance of different sensors showed that each device performed differently when compared with Pyranometer. The underestimates the irradiance with median error bias by -5 W/m^2 (-3 %), respectively. For , the bias error is -1 W/m^2 which is significantly lower. The error range for is -8 W/m^2 to 8 W/m^2 (-5% to 5%). Among all the sensors, has the highest bias error and error range. The error underestimates the irradiance with error ranging from -8 W/m^2 to 22 W/m^2 (-2% to 6%) with a bias of 6 W/m^2. The 8 months of data were separated for varying environmental conditions (Summer and winter months). The device performance is quite similar during both summer and winter months with error range of -18 W/m^2 to 8 W/m^2 (-8% to 3%) and -8 W/m^2 to 2 W/m^2 (-10% to 2%). The sensor data had excessive outliers. The removal of these outliers shrunk the dataset resulting in low relative error. The performance of the device is not uniform in the summer and winter months. The bias error is almost negligible for sensor during summer months (> -1W/m^2, >1%), but has a slightly higher relative bias (2.5%) in winter months. During winter months the error range, bias errors are low due to low irradiance which reduces the error in the data. The error distribution was not uniform but the range of relative distribution only differed slightly.

The irradiance sensors behavior is similar to pyranometers during low Air mass . The sensors underestimate or overestimate when the Air mass is high. The deviation of PV reference cell ( ) from Pyranometer is highest among all other instruments. The sensor agreed with the Pyranometer output in the most of the period. The irradiance devices are sensitive to the spectral composition of sunlight due to variation in calibration environments which also causes deviation among instruments [41]. The empirical correction factors or normalization factor is implemented to correct the response of sensors. The empirical correction factor of 1.005,1.008,1.012, and 0.9746 can be applied to respectively. The graphs of linear fit for all the sensors are shown in figure 5.6. These correction factor changes with the location due to different environmental conditions. The calibration excellency of the device is also shown by the following graph. The correction is only applicable in Delft, The Netherlands.

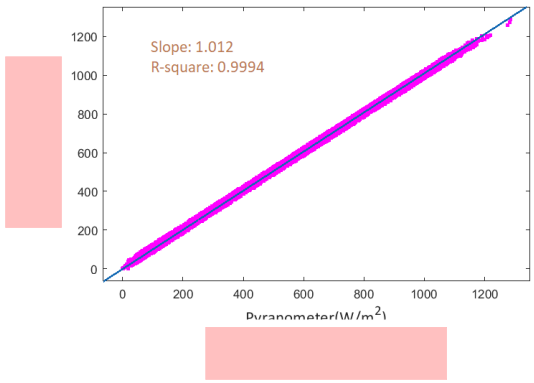

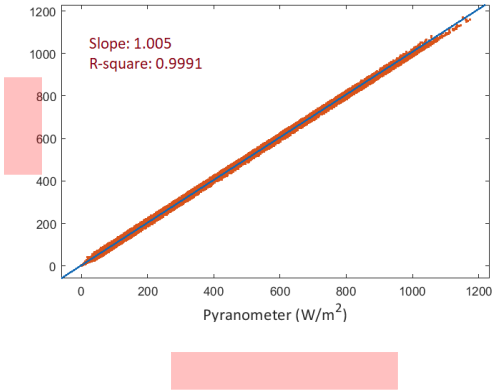

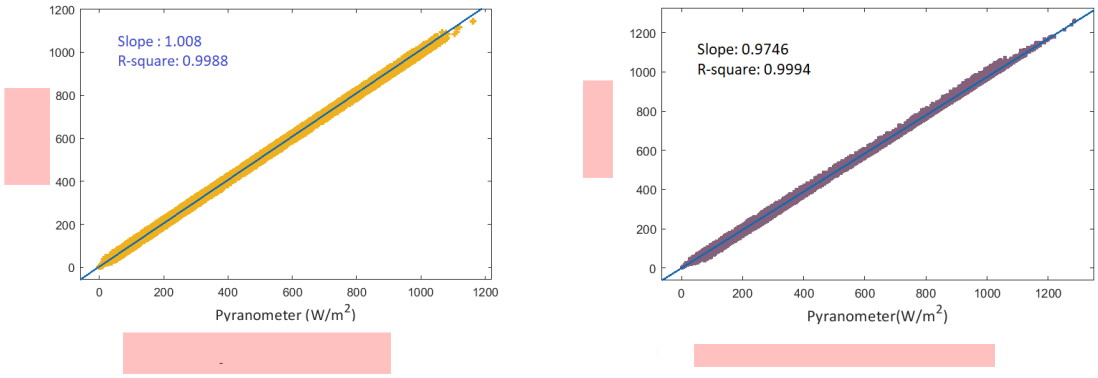

Figure 5.6: Linear fit Pyranometer vs cost-effective sensors

The above results were evaluated based on 1-minute data for 8 months. The results can improve if evaluated with more datasets. The test should be conducted in different environmental conditions to check the demonstrability of results.

In the next chapter, the artificial intelligence algorithm used to improve the output of cost-effective sensor will be introduced.

6

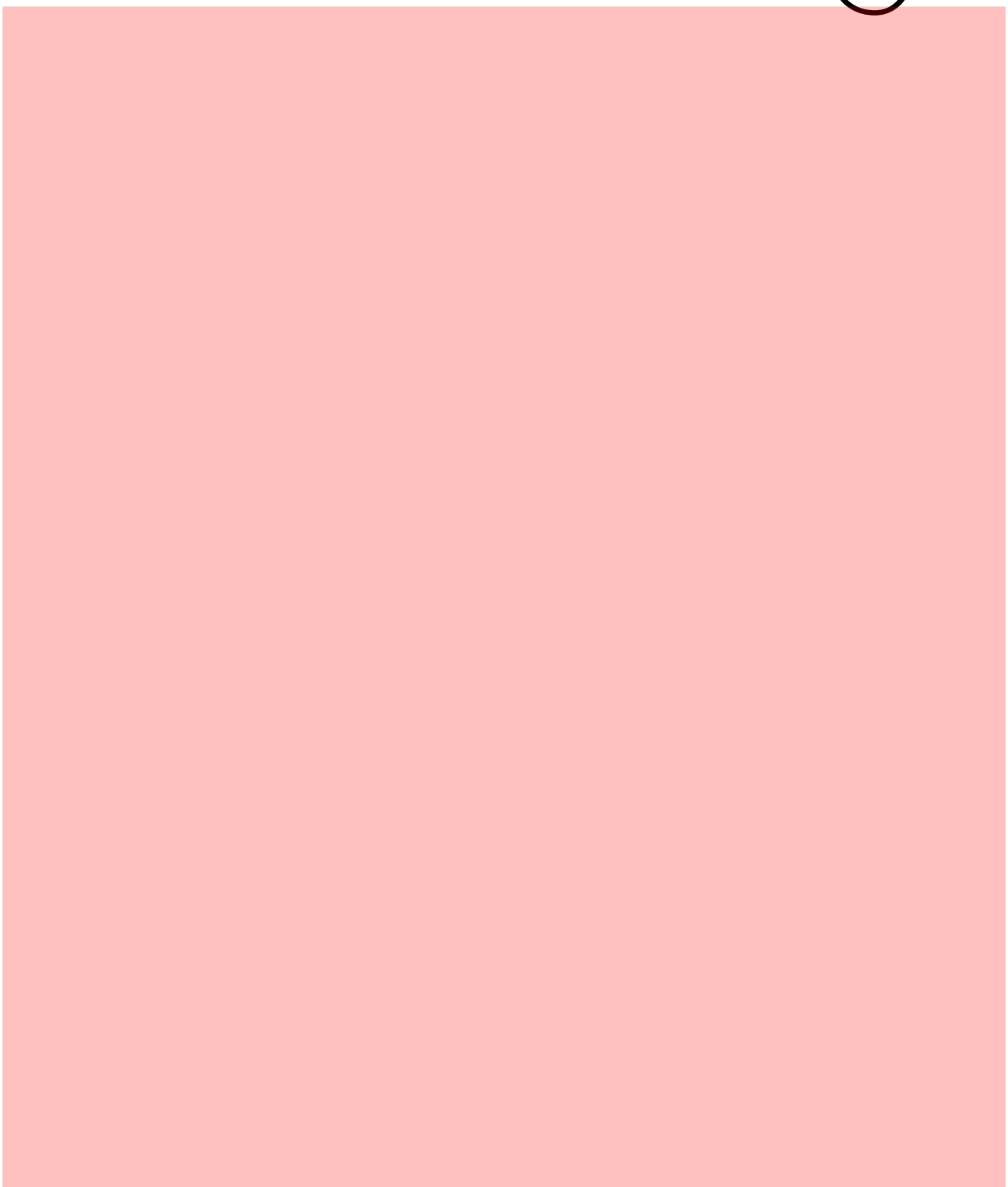

7

Conclusions & Recommendations

7.1. Conclusions

1. **What is the procedure to develop a primary reference cell?**

   The ASTM E1125 standard was studied in order to develop a Primary PV Reference cell. The PV reference cell should be calibrated in natural sunlight. The temperature of the PV cell should be maintained at 25°C with irradiance between 750 W/m^2 to 1000 W/m^2. The PV cell field of view should be same as pyrheliometer during the calibration. The mechanical housing was designed according to World photovoltaic standard and manufactured in Kipp & Zonen D& E department. The PV cell was characterized in the TU Delft Laboratory. The PV cell fulfills all the characterization standards. Finally, the reference cell was assembled and calibrated in Almeria, Spain.

2. **Can Dust IQ PV module become a reference cell? If so, by which design or method?**

   Yes, Mini-PV modules can be calibrated as a PV reference cell. Due to the PV module size, the Module cannot be calibrated as a Primary Reference cell. The collimator design is not possible for a PV module in DUSTIQ as it does not match with the standards. The module can be calibrated as a Secondary Reference cell. For this Kipp & Zonen should either make their own solar simulator or purchase it. The alternative option can be designing a cooling unit for calibrating it in LASS solar simulator in TU Delft Laboratory. The calibration transfer can be done within 10 seconds if the LASS temperature does not rise beyond 25°C quickly.

3. **How are the cost-effective sensors performing when compared with pyranometer?**

   The 8 months of data collected from different cost-effective sensors were compared with Pyranometer data. All the sensors were placed in the same plane of the array. The overall performance of different sensors showed that each device performed differently when compared with Pyranometer. The underestimates the irradiance with median error bias by -5 W/m^2 (-3%), respectively. For , the bias error is -1 W/m^2 which is significantly lower. The error range for is -8 W/m^2 to 8 W/m^2 (-5% to 5%). Among all the sensors, the had the largest bias error and error range. The error overestimates the irradiance with error ranging from -8 W/m^2 to 22 W/m^2 (-2% to 6%) and bias of 6 W/m^2. The was closest with the calibration standard of Pyranometer. The PV reference cell from was had the error among all the instruments. This results makes it likely that this reference cell is at most a simple working class reference cell.
   The comparison of the cost-effective sensor in varying Air mass with regards to Pyranometer exhibited

that Silicon Pyranometer performance was close to Pyranometer during altering Air mass. The PV reference cell underestimated irradiance reading during the evening and morning hours when the Air mass is high. The Silicon Pyranometer ( ) was similar to Pyranometer irradiance reading during different Airmass making it the most accurate cost-effective sensor.

4. **How accurate is the DustIQ data in contrast to other PV reference cell?**

   The bias error of the DustIQ is better considering silicon sensor bias error. The expanded error distribution ranges from -15 W/m^2 to 25 W/m^2 (-12% to 10%),and bias error for DustIQ PV cells is 4W/m^2 (2%). The has error ranging from -8 W/m^2 to 22 W/m^2 (-2% to 6%) and bias of 6 W/m^2. The statistical errors RMSE and MAE of DusiIQ is 19 W/m^2 to 13 W/m^2 vs 14 W/m^2 and 9 W/m^2 respectively. The statistical error is slightly higher for DustIQ PV module compared to the silicon sensor which can be due to a large area of the Mini-PV module compared to the small area of reference cell. Therefore, the performance of DustIQ PV module can better silicon sensor if calibrated according to high standards

7.2. Recommendations

Regardless of all the research work accomplished, there are room for improvements for further research. Some recommendations for future work are:

- **Validate the performance of Primary reference cell with respect to Pyranometer.**
  The newly developed Primary Reference from Kipp & Zonen should be compared with Thermopile Pyranometer data to check its accuracy. The Pyranometer from Kipp & Zonen is considered to be one of the best irradiance sensor available. The performance ratio between two sensors will give an upright understanding of Primary reference cell accuracy.
- **Investigate on procedure to develop a solar simulator to calibrate Mini PV module in DustIQ.**
  The class AAA solar simulator is required to calibrate Mini PV module in DustIQ as a Secondary Reference cell. It will be economical for Kipp & Zonen to develop their own solar simulator to calibrate the PV module in large scale.

Bibliography

[1] Unfccc, "ADOPTION OF THE PARIS AGREEMENT - Paris Agreement text English," Tech. Rep. [Online]. Available: https://unfccc.int/sites/default/files/english{_}paris{_}agreement.pdf

[2] EMILIANO BELLINI, "Dubai: Tariff for large-scale PV hits new low at $0.024/kWh – pv magazine International," 2018. [Online]. Available: https://www.pv-magazine.com/2018/11/05/dubai-tariff-for-large-scale-pv-hits-new-low-at-0-024-kwh/

[3] IEA PVPS, "Snapshot of Global PV Market," vol. 1, p. 43, 2019.

[4] Y. Jestin and S. Cell, "Photovoltaic Solar Energy Learn more about Solar Spectra Solar Spectra."

[5] "CMP series • Pyranometer CMA series • Albedometer Instruction Manual," Tech. Rep., 2016. [Online]. Available: www.kippzonen.com

[6] "A new way of monitoring commercial rooftop PV Designed," Kipp & Zonen, Tech. Rep., 2018. [Online]. Available: www.kippzonen.com/rt1

[7] "Solar Reference Cell — Solarmer." [Online]. Available: http://solarmer.com/solar-reference-cell

[8] W.vanSark, N.Reich, B.Müller, A.Armbruster, and K.Kiefer, "Review of PV Performance Ratio Development," no. 6, 2012.

[9] S.Karki and S.Ramesh, "PV Modules Task 3 4/5/2018," Tech. Rep., 2018.

[10] A.Smets, O.Isabella, K.Jäger, R. Swaaij, and M. Zeman., *Solar energy : the physics and engineering of photovoltaic conversion, technologies and systems*. UIT Cambridge, 2016.

[11] "Effect of Temperature | PVEducation." [Online]. Available: https://www.pveducation.org/pvcdrom/solar-cell-operation/effect-of-temperature

[12] M. R. Maghami, H. Hizam, C. Gomes, M. A. Radzi, M. I. Rezadad, and S. Hajighorbani, "Power loss due to soiling on solar panel: A review," pp. 1307–1316, jun 2016.

[13] J. Zorrilla-Casanova, M. Piliougine, J. Carretero, P. Bernaola, P. Carpena, L. Mora-Lopez, and M. Sidrach-de Cardona, "Analysis of Dust Losses in Photovoltaic Modules," pp. 2985–2992, 2011. [Online]. Available: http://www.ep.liu.se/ecp/article.asp?issue=057{%}26volume=11{%}26article=39

[14] P. Nepal, "Effect of Soiling on the PV Panel kWh Output," Ph.D. dissertation, Delft University of Technology, 2018. [Online]. Available: http://repository.tudelft.nl/.

[15] M. Mani and R. Pillai, "Impact of dust on solar photovoltaic (PV) performance: Research status, challenges and recommendations," 2010.

[16] M. Korevaar, J. Mes, A. A. Merrouni, T. Bergmans, P. Nepal, and X. Van Mechelen, "Unique soiling detection system for PV modules," Tech. Rep.

[17] Y. J. Wang and P. C. Hsu, "An investigation on partial shading of PV modules with different connection configurations of PV cells," *Energy*, 2011.

[18] E. D. Dunlop, "Lifetime performance of crystalline silicon PV modules," *3rd World Conference on Photovoltaic Energy Conversion*, no. September, pp. 2928–2930, 2003.

[19] "Shade Losses in PV Systems, and Techniques to Mitigate Them." [Online]. Available: https://blog.aurorasolar.com/shading-losses-for-pv-systems-and-techniques-to-mitigate-them/

[20] "PV Power Loss Due to Snow On Panels." [Online]. Available: https://www.builditsolar.com/Projects/PV/EnphasePV/SnowOnPV.htm

[21] “Standard Specification for Physical Characteristics of Nonconcentrator Terrestrial Photovoltaic Reference Cells 1.” [Online]. Available: http://www.copyright.com/

[22] “Designation: E1125 16 Standard Test Method for Calibration of Primary Non-Concentrator Terrestrial Photovoltaic Reference Cells Using a Tabular Spectrum 1.” [Online]. Available: www.astm.org,

[23] K. A. Emery, “Pyranometers and refer- ence cells , the difference,” no. April 2012, 2016.

[24] Iec, “IEC 60904-2 INTERNATIONAL STANDARD NORME INTERNATIONALE Photovoltaic devices-Part 2: Requirements for photovoltaic reference devices Dispositifs photovoltaïques-Partie 2: Exigences applicables aux dispositifs photovoltaïques de référence,” Tech. Rep., 2015. [Online]. Available: www.iec.ch

[25] “Designation: E1362 15 Standard Test Methods for Calibration of Non-Concentrator Photovoltaic Non-Primary Reference Cells 1.” [Online]. Available: www.astm.org,

[26] Heraeus Nexensos USA, “Wirewound Glass,” 2019. [Online]. Available: https://www.heraeus.com/en/hne/sensor{_}products/wirewound{_}glass/wirewound{_}glass.html

[27] Kipp & Zonen, “Cables and Connections - Kipp & Zonen.” [Online]. Available: https://www.kippzonen.com/Knowledge-Center/Cables-and-Connections

[28] UQG OPTICS, “Fused Silica Spectosil Optical Materials - UQG Optics.” [Online]. Available: https://www.uqgoptics.com/materials{_}optical{_}spectosil.aspx

[29] C. R. Osterwald, S. Anevsky, A. K. Barua, P. Chaudhuri, J. Dubard, K. Emery, B. Hansen, D. King, J. Metzdorf, F. Nagamine, R. Shimokawa, Y. X. Wang, T. Wittchen, W. Zaaiman, A. Zastrow, and J. Zhang, “The World Photovoltaic Scale: An International Reference Cell Calibration Program,” Tech. Rep., 1997.

[30] Ben’s Electronics, “Peltier element 60 Watt - www.benselectronics.nl.” [Online]. Available: https://benselectronics.nl/peltier-element-60-watt/?gclid=EAIaIQobChMIkILv2Mno4gIVEc53Ch17Sgc4EAQYAiABEgKRk{_}D{_}BwE/

[31] “Course | PV2x | edX,” 2019. [Online]. Available: https://courses.edx.org/courses/course-v1:DelftX+PV2x+1T{_}2018/course/

[32] S. Yang, “Optical detector nonlinearity :,” National Bureau of Standards, Gaithersburg, MD, Tech. Rep., 1995. [Online]. Available: https://nvlpubs.nist.gov/nistpubs/Legacy/TN/nbstechnicalnote1376.pdf

[33] “The PMO6-cc radiometer – Davos Instruments.” [Online]. Available: http://davos-instruments.ch/products/the-pmo6-cc/

[34] Kipp and Zonen, “KippZonen_CHP1_Pyrheliometer_Manual_0901,” Tech. Rep., 2008. [Online]. Available: www.kippzonen.com

[35] “Learn more online at www.oceanoptics.com Contact an Ocean Optics Application Scientist for details and pricing,” Tech. Rep. [Online]. Available: www.oceanoptics.com

[36] Kipp and Zonen, “Instruction Manual 2 AP 2-Axis Sun Tracker / Positioner Gear Drive,” Tech. Rep., 2005. [Online]. Available: www.kippzonen.com

[37] “AAA class steady state solar simulator - Eternal Sun.” [Online]. Available: http://www.eternalsun.com/products/solar-simulator/

[38] Z. Jin, W. Yezheng, and Y. Gang, “General formula for estimation of monthly average daily global solar radiation in China,” *Energy Conversion and Management*, 2005.

[39] F. Kasten, A. T. Young, A. Young, and A. Young, “Revised optical air mass tables and approximation formula,” *Applied Optics*, vol. 28, no. 22, p. 4735, nov 1989. [Online]. Available: https://www.osapublishing.org/abstract.cfm?URI=ao-28-22-4735

[40] E. Laue, “The measurement of solar spectral irradiance at different terrestrial elevations,” *Solar Energy*, vol. 13, no. 1, pp. 43–57, apr 1970. [Online]. Available: https://linkinghub.elsevier.com/retrieve/pii/0038092X7090006X

[41] P. M. Sengupta, P. Gotseff, and T. Stoffel, "Evaluation of Photodiode and Thermopile Pyranometers for Photovoltaic Applications: Preprint," Tech. Rep., 2012. [Online]. Available: http://www.osti.gov/bridge

[42] A. de Montgareuil, J.-L. Martin, F. Mezzasalma, and J. Merten, "Main results of the first intercomparison campaign of European irradiance sensors at INES Cadarache (2007)," jun 2007.

[43] A. Zamaniyan, F. Joda, A. Behroozsarand, and H. Ebrahimi, "Application of artificial neural networks (ANN) for modeling of industrial hydrogen plant," *International Journal of Hydrogen Energy*, vol. 38, no. 15, pp. 6289–6297, may 2013.

[44] R.Rojas, "The Backpropagation Algorithm 7.1 Learning as gradient descent," Springer-Verlag, Tech. Rep., 1996.

[45] T. L. Lee, "Back-propagation neural network for long-term tidal predictions," *Ocean Engineering*, vol. 31, no. 2, pp. 225–238, 2004.

[46] J.Portilla, "A Beginner's Guide to Neural Networks in Python | Springboard Blog," 2017. [Online]. Available: https://www.springboard.com/blog/beginners-guide-neural-network-in-python-scikit-learn-0-18/

A

Mechanical housing design of PV Reference cell

The design of PV reference cell from Kipp & zonen compiles with the WPVS standard.The detailed figure of the mechanical housing of the PV reference cell with the dimensions is given below.

B

Relative Errors

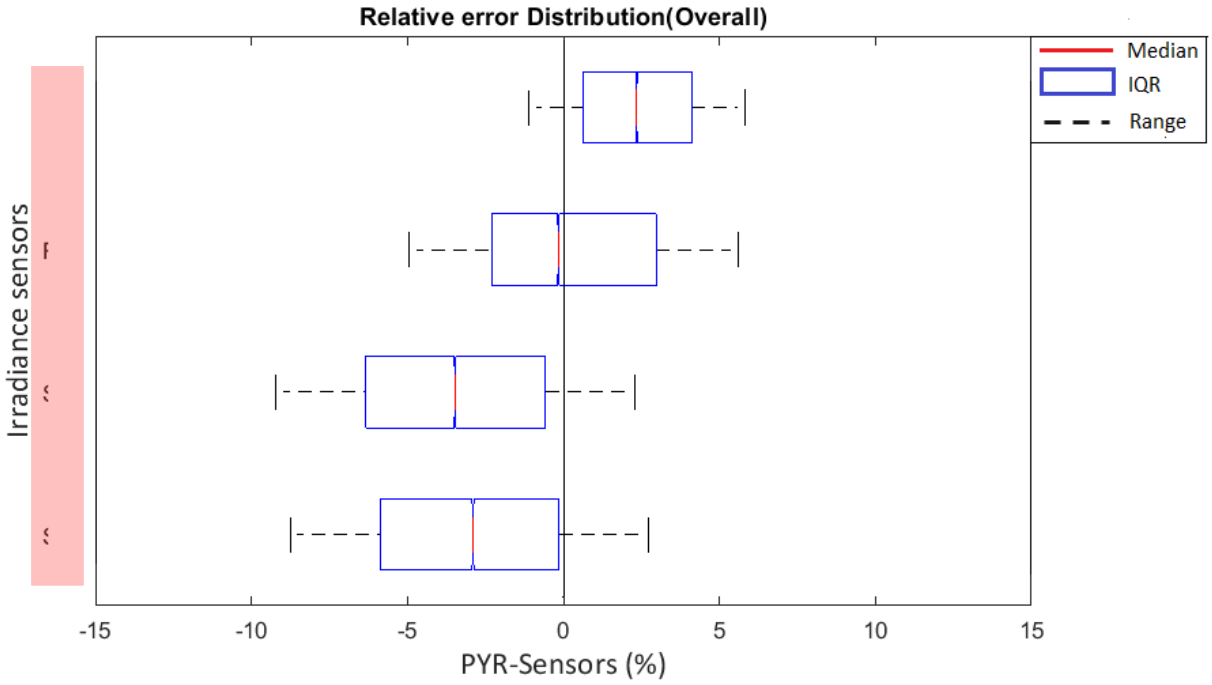

Figure B.1: Overall Relative error distribution

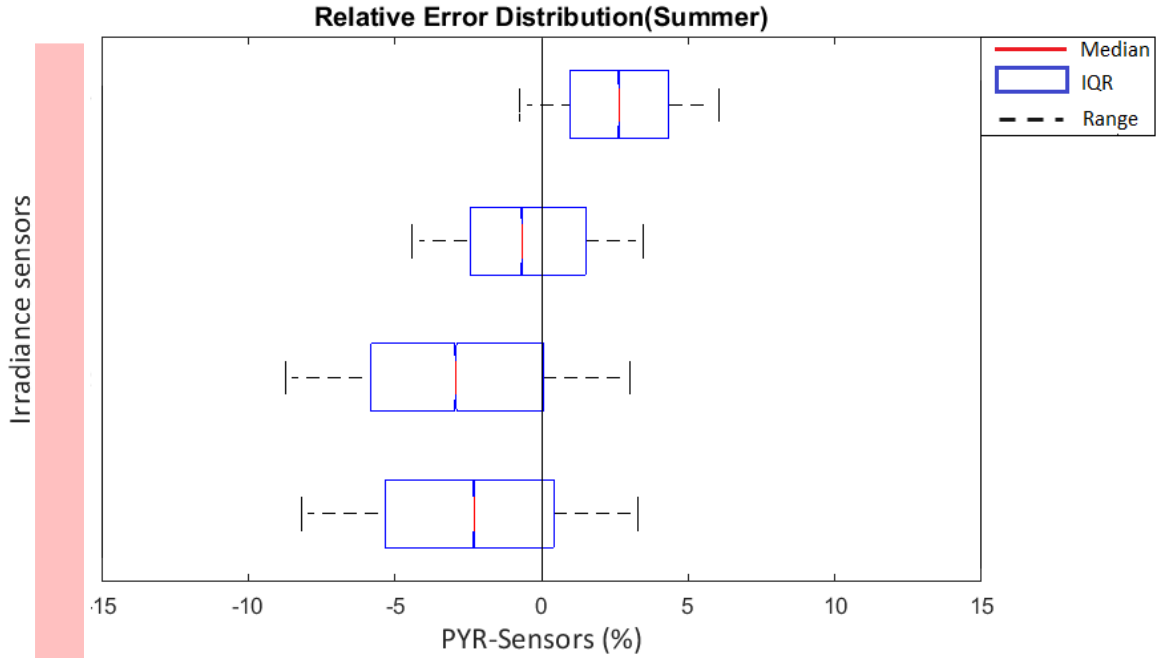

(a) Overall Relative Error distribution

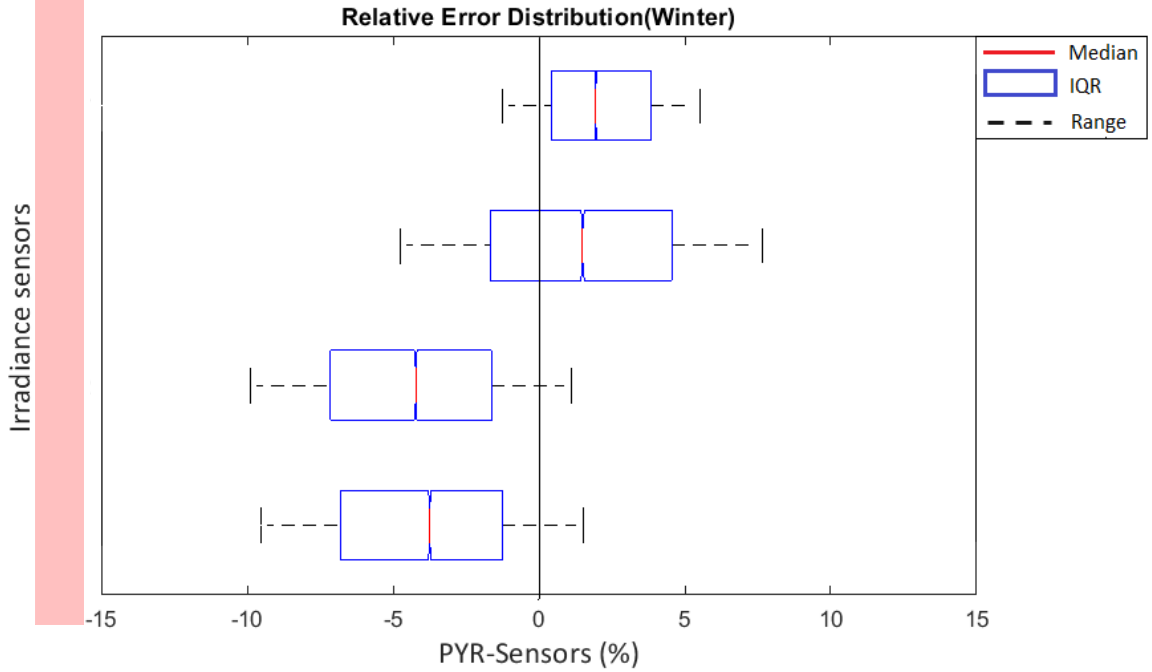

(b) Relative Error distribution during summer

Figure B.2: Boxplot diagrams of the Relative error distributions at different conditions.

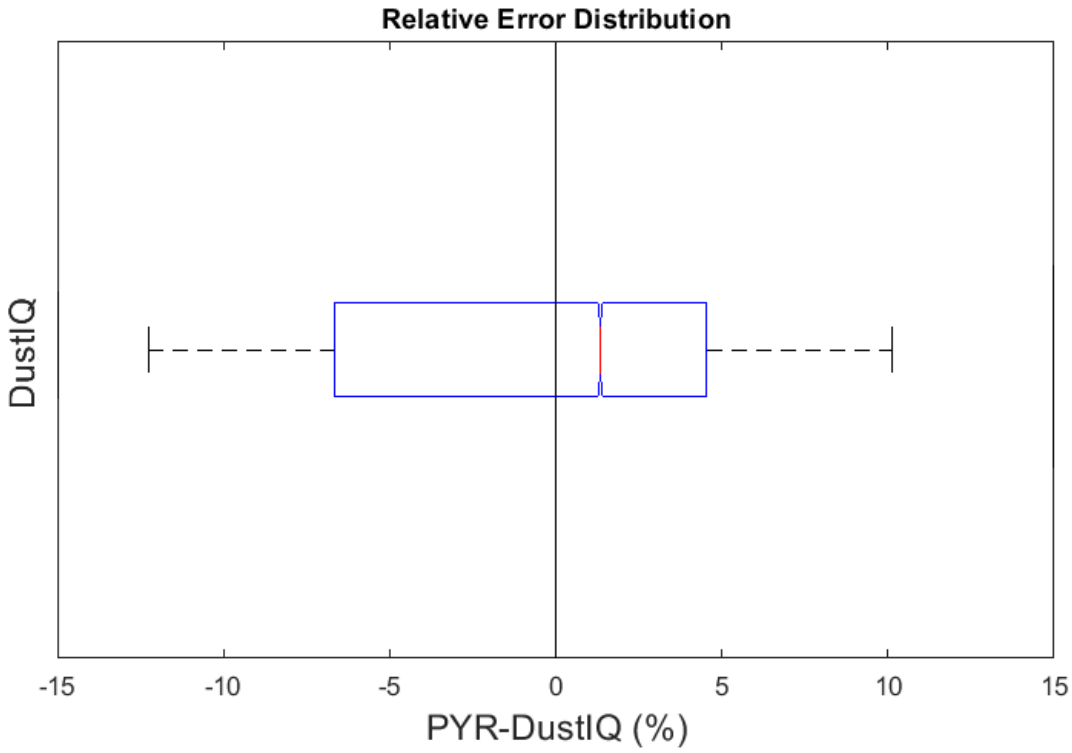

Figure B.3: Overall Relative error distribution between Pyranometer and DustIQ

C

Glossary

C.1. Acronyms

ASTM	American Society for Testing and Materials
C-Si	Crystalline silicon
CV	Calibration value
DC	Direct Current
DHI	Diffuse Horizontal Irradiance
DNI	Direct Normal Irradiance
EQE	External Quantum Efficiency
EVA	Ethylene-vinylacetate
FOV	Field of view
FF	Fill Factor
GHI	Global Horizontal Irradiance
IQR	interquartile range
IEA	International Energy Agency
IEC	International Electrotechnical Commission
LASS	Large Area Steady State Solar Simulator
LED	Light Emitting Diode
MT	Mencke & Tegtmeyer
MAPE	Mean Absolute Percentage Error
MPP	Maximum Power Point
MPPT	Maximum Power Point Tracking

NL Non- Linearity

OSM Optical soiling technology measurement

OC Open Circuit

OD Optical Density

PVC Polymerization of vinyl chloride

POA Plane Of Array

PR Performance Ratio

PV Photovoltaic

PVMD Photovoltaic Material and Devices

RTDs Resistance temperature detectors

RMSE Root Mean Square Error

SC Short Circuit

SF Shading Factor

SR Soiling Ratio

STC Standard Test Condition

SVF Sky View Factor

UV Ultra-Violet

WPVS World photovoltaic scale

C.2. List of Symbols

α	Temperature coefficient for short-circuit current
β	Temperature coefficient for open-circuit voltage
I_{SC}	Short-circuit current
V_{OC}	Open-circuit voltage
P_{MPP}	Maximum power
I_{MPP}	Maximum current
V_{MPP}	Maximum voltage
η	Efficiency
J_0	Saturation current density
λ_0	Longitude of observer
θ_S	Slope angle
x	Aperture stop
θ_O	Opening angle
A_S	Azimuth of the Sun
α	Temperature coefficients
β	Proportionality constant
∇_{NL}	Non-linearity
λ	Wavelength
$\phi(\lambda)$	Spectral photon flux
$\Theta_D(\lambda)$	Partial derivative of quantum efficiency
$Z_P(\lambda)$	Spectral transmittance
$Q_D(\lambda, T_0)$	Quantum efficiency
β	Learning rate
δ_j	Error signal